

COOLING PERFORMANCE INVESTIGATION OF A TWO-PASS RIB-
ROUGHENED CHANNEL

A THESIS SUBMITTED TO
THE GRADUATE SCHOOL OF NATURAL AND APPLIED SCIENCES
OF
MIDDLE EAST TECHNICAL UNIVERSITY

BY

İSA KAVAS

IN PARTIAL FULFILMENT OF THE REQUIREMENTS
FOR
THE DEGREE OF MASTER OF SCIENCE
IN
AEROSPACE ENGINEERING

AUGUST 2015

Approval of the thesis:

**COOLING PERFORMANCE INVESTIGATION OF A TWO-PASS
RIB-ROUGHENED CHANNEL**

Submitted to **İSA KAVAS** in partial fulfilment of the requirements for the degree of **Master of Science in Aerospace Engineering Department, Middle East Technical University** by,

Prof. Dr. GÜLBİN DURAL ÜNVER _____
Dean, Graduate School of **Natural and Applied Sciences**

Prof. Dr. OZAN TEKİNALP _____
Head of Department, **Aerospace Engineering**

Assoc. Prof. Dr. DİLEK FUNDA KURTULUŞ _____
Supervisor, **Aerospace Engineering Dept., METU**

Examining Committee Members

Prof. Dr. OZAN TEKİNALP _____
Aerospace Engineering Dept., METU

Assoc. Prof. DİLEK FUNDA KURTULUŞ _____
Aerospace Engineering Dept., METU

Asst. Prof. Dr. ALİ TÜRKER KUTAY _____
Aerospace Engineering Dept., METU

Prof. Dr. ALTAN KAYRAN _____
Aerospace Engineering Dept., METU

Assoc. Prof. Dr. MUNİR ELFARRA _____
Flight Training Department, University of Turkish Aeronautical Association

Date: 28/08/2015

I hereby declare that all information in this document has been obtained and presented in accordance with academic rules and ethical conduct. I also declare that, as required by these rules and conduct, I have fully cited and referenced all material and results that are not original to this work.

Name, Last name : İsa Kavas

Signature :

ABSTRACT

COOLING PERFORMANCE INVESTIGATION OF A TWO-PASS RIB-ROUGHENED CHANNEL

Kavas, İsa

M.S., Department Of Aerospace Engineering

Supervisor: Assoc. Prof. Dr. Dilek Funda Kurtuluş

Co-Supervisor: Dr. Tolga Yasa

August 2015, 79 Pages

The performance of the modern aero-engines is highly dependent on the turbine inlet gas temperature. The higher temperature leads to more compact and efficient machines. Additionally, specific fuel consumption of the engine is decreased for the same thrust rating. However, the turbine inlet temperatures of the today's engines are already beyond the material structural limits. Hence, the turbine section must be cooled down to acceptable levels.

Various types of cooling methods are typically applied to the gas turbine blades like internal cooling, film cooling, impingement cooling etc. The internal cooling channels are embedded inside the turbine blades and often equipped by ribs in order to enhance the turbulence activities and heat transfer area. Cooling channels may form as a single pass or multi-pass channels depending on the design considerations. Current research focuses on

experimentally and numerically investigating the thermal performance of a 2-pass channel. Especially the performance of U turn section and its effect on the second channel were studied.

A rectangular cross section tunnel with two passage and a U-turn section that mimic the modern gas turbine cooling configurations was designed and manufactured. The ribs with square cross section are located on the bottom wall of both passages. The ambient air is sucked to the wind tunnel by using a blower. The bottom wall of the test section was heated by a foil heater which generates uniform heat flux. The wall surface temperature was obtained by means of optical thermography method (IR camera). The heat loss was computed assuming one-dimensional heat conduction through the wall. The experiments were conducted at three Reynolds number by changing the blower speed. Finally the Nusselt number was computed based on the heater power, surface temperature and the mainstream temperature. The results were compared with the smooth wall configuration.

The current investigation aims to provide Nusselt numbers and deep understanding of the flow physics of the modern gas turbine cooling configuration both experimentally and numerically. The U-turn section and cooling passage interaction is investigated. The cooling effectiveness improvement by design is addressed at the end of the manuscript. Experimental results are compared with the numerical analysis to come up with a suitable turbulence model.

ÖZ

U DÖNÜŞLÜ KANALDA SOĞUTMA PERFORMANSI ARAŞTIRMASI

Kavas, İsa

Yüksek Lisans., Havacılık ve Uzay Mühendisliği Bölümü

Tez Yöneticisi: Doç. Dr. Dilek Funda Kurtuluş

Yardımcı Tez Yöneticisi: Dr. Tolga Yasa

Ağustos 2015, 79 Pages

Modern gaz türbinli motorların performansı türbin giriş sıcaklığına yüksek derecede bağlıdır. Yüksek sıcaklık daha kompakt ve verimli makineler sağlar. Buna ek olarak, aynı itki seviyesinde motorun özgül yakıt sarfiyatı azalır. Ancak, günümüz motorlarında türbin giriş sıcaklıkları malzeme dayanım limitlerinin üzerindedir. Sonuç olarak, türbin bölgesi kabul edilebilir seviyelere soğutulmalıdır.

İç soğutma, film soğutma çarpmalı jetle soğutma gibi çeşitli tiplerde soğutma yöntemleri türbin palelerine uygulanır. Türbin palelerinin içerisine soğutma kanalları tasarlanır ve bu kanallar sıklıkla ısı transferi alanını ve kanal içi türbülans aktivitelerini artırıcı engeller içerir. Soğutma kanalları tasarım anlayışına bağlı olarak tek geçişli veya çok geçişli halde bulunabilir. Mevcut çalışma 2 geçişli bir kanalın termal performansını deneysel ve hesaplamalı akışkanlar dinamiği analizleri ile incelemek üzere yoğunlaşmıştır. Özellikle U dönüş bölgesi performansı ve devamındaki bölgeye etkileri çalışılmıştır.

Gaz türbin soğutma konfigürasyonunu taklit eden, kare kesitli U dönüş içeren 2 geçişli bir tünel tasarlanıp üretilmiştir. 2 kanalda da alt yüzeye kare kesitli engeller yerleştirilmiştir. Fan yardımıyla ortam havası tünel içine emilmektedir. Tünel test bölgesi alt yüzeyi sabit ısı akısı sağlayan folyo ısıtıcı ile ısıtılmıştır. Yüzey sıcaklık dağılımları ısı görüntüleme (infrared kamera) yöntemiyle elde edilmiştir. Alt duvardan ısı kayıpları bir-boyutlu ısı iletimi varsayımı ile hesaplanmıştır. Fan ayarı değiştirilerek üç Reynolds sayısında deneyler yapılmıştır. Son olarak, ısıtıcı gücü, ısıtılan yüzey ve akış sıcaklığı kullanılarak Nusselt sayısı hesaplanmaktadır. Sonuçlar pürüzsüz kanal konfigürasyonu ile karşılaştırılmıştır.

Mevcut çalışma modern gaz türbinli motor soğutma konfigürasyonlarında deneysel ve numeric olarak Nusselt sayılarının elde edilmesini ve akış fiziğinin derinlemesine anlaşılmasını amaçlamaktadır. U dönüş ve düz kanal etkileşimi araştırılmıştır. Çalışma sonunda tasarımda soğutma etkinliği iyileştirmesine değinilmiştir. Uygun türbülans modeli ortaya koymak amacıyla deneysel sonuçlar hesaplamalı akışkanlar dinamiği analizi sonuçları ile karşılaştırılmıştır.

To my family and Elif...

ACKNOWLEDGEMENTS

I would like to extend my deepest gratitude to my advisor Assoc. Prof. Dr. Dilek Funda KURTULUŞ and my coadvisor Dr. Tolga YASA for their help, guidance, advice, criticism and encouragements throughout the study.

I would like to thank TUSAS ENGINE INDUSTRIES which involved me as a researcher for RBF4 AERO 7th framework EU project since the studies in this thesis is a part of the this program.

I am thankful to my colleagues Çağrı NART, Ender HEPKAYA, Görkem ÖZTARLIK, Samet ASLAN, Sefa YILMAZTÜRK, Yavuzer KARAKUŞ, Sinan İNANLI, Gözde ERGÜN, Bekir Berdan AKSOY, Bertan KAYNAROĞLU, İlhan GÖRGÜLÜ, Feridun KUŞÇU, Emrah DAŞİK, Taner YAVAŞ, Muhittin ARSLAN, Turgay KARAKUŞ, Celal BORA, Eyüp ERGÜT, Hüseyin BIÇAKÇI, İsmail GÜLGÜN, Volkan GÜRAKAN, Lütfi ŞEN, Ali KARAKUŞ, Gökay GÜNAÇAR and my old friends Alper ÇELİK and Doğan POYRAZ for supporting of my thesis.

I owe special and deepest gratitude to my family Cahide KAVAS, Osman KAVAS, Ebru KAVAS and Elif ALTUNTOP for their friendship, love, support, patience and encouragement throughout the study.

TABLE OF CONTENTS

ABSTRACT.....	V
ÖZ	VII
ACKNOWLEDGEMENTS.....	X
TABLE OF CONTENTS.....	XI
CHAPTERS	1
1. INTRODUCTION	1
1.1. Turbine Internal Cooling	7
1.1.1. Ribbed Channel Flow	8
1.2. Motivation.....	17
2. EXPERIMENTAL PROCEDURE	19
2.1. Design of the Experimental Setup	19
2.2. Instrumentation and Measurement Techniques	24
2.2.1. Air Velocity and Temperature Measurements.....	24
2.2.2. Heating the model.....	27
2.2.3. Temperature Measurements.....	29
2.2.4. Test Procedures	32
2.2.5. Uncertainty Analysis.....	34
3. NUMERICAL SETUP	37
3.1. Model Geometry and Boundary Conditions.....	37
3.2. Turbulence Modeling.....	40
3.2.1. Realizable k- ϵ model.....	42

3.2.2. Low Reynolds Yang-Shih Model.....	44
3.2.3. v2f Model	45
3.2.4. k- ω -SST Model	45
3.2.5. Reynolds Stress Models	47
3.3. Numerical Approach and Mesh Generation.....	48
4. HEAT TRANSFER RESULTS AND DISCUSSION	53
4.1. Heat Transfer in Smooth and Ribbed Channels	53
4.2. Comparison with Numerical Predictions	59
4.3. Discussion and Conclusion	67
4.4. Future Work	70
REFERENCES.....	71
APPENDIX.....	77

LIST OF TABLES

Table 1.1 Turbine blade materials [3].....	3
Table 2.1 Sensitivities of Nusselt number for Re=20000 case	36
Table 2.2 Uncertainties of Nusselt number for Re=20000 case	36
Table 3.1 Number of nodes for mesh generation (ribbed case).....	52

LIST OF SYMBOLS

A	Heated surface area
AR	Aspect ratio
CFD	Computational fluid dynamics
c_p	Specific heat
De	Dean number
deg	Degree
D_h	Hydraulic diameter
e	Rib height
e/D_h	Rib height to hydraulic diameter
Ec	Eckert number
EXP	Experimental
EXP_R	Experimental results for ribbed case
EXP_S	Experimental results for smooth case
h	Convective heat transfer coefficient
H	Height of channel
I	Amper
IR	Infra red
k	Thermal conductivity
K	Kelvins
k_{air}	Thermal conductivity of air
k_p	Thermal conductivity of plexiglass
LES	Large eddy simulation
Nu	Nusselt number
Nu_{sm}	Nusselt number for smooth wall
ORS	Omega Reynolds stress
P	Rib pitch
p	pressure

P	Rib pitch
P/e	Rib pitch to rib height ratio
Pa	Pascals
PIV	Particle image velocimetry
Pr	Prandtl number
PS	Pressure sector
q	Heat flux
q _{loss}	Heat flux for losses
R	Universal gas constant
R	Radius of curvature
RANS	Reynolds averaged Navier Stokes
Re	Reynolds number
RKE	Realizable k-epsilon model
RSM	Reynolds Stress Model
SST	Shear stress transport
T	Temperature
T _g	Air bulk temperature
T _m	Mean temperature
TS	Temperature sector
T _{tc}	Temperature of loss thermocouples
T _w	Heated wall surface temperature
U _m	Mean velocity
U _m	Mean velocity
V	Volt
W	Work output
W	Width of channel
y ⁺	Dimensionless wall distance
YS	k-ε Yang Shih Model
γ	Ratio of specific heat of a gas
ΔT	Temperature difference

μ	Dynamic viscosity
ρ	Density

LIST OF FIGURES

Figure 1.1 Open Gas Turbine Cycle	1
Figure 1.2 Evolution of the turbine entry temperature (TET) capability of Rolls-Royce's civil aeroengines, from 1940 to the present day [4]	4
Figure 1.3 Cooling applied blade[5]	5
Figure 1.4 Channel with ribs on one wall, side view (left), top view (right).....	7
Figure 1.5 Secondary flows due to 45deg ribs[15]	10
Figure 1.6 Rib shape and rib cross-section examples	11
Figure 1.7 Rotating blade and internal channels.....	14
Figure 2.1 Experimental setup	21
Figure 2.2 Experimental facility	21
Figure 2.3 Tunnel description (top view)	22
Figure 2.4 Test section.....	23
Figure 2.5 Rib geometry (side view)	23
Figure 2.6 Measurement Sectors of Test section	24
Figure 2.7 Air temperature estimation along the channel model.....	25
Figure 2.8 Flow measurement probes	25
Figure 2.9 Probe instrumentation at inlet(upper) and outlet(lower)(not to scale)	27
Figure 2.10 Tunnel heating	28
Figure 2.11 Inconel foil heating composite (not to scale)	28
Figure 2.12 Photos(top) and temperature contours(bottom) of the heater decision study....	29
Figure 2.13 Internal (left) and external (right) thermocouple locations	30
Figure 2.14 Temperature and pressure calibration examples	31
Figure 2.15 Transmissivity of the infrared window	31
Figure 2.16 Post processing algorithm	34
Figure 3.1 Top view and 3D view of numerical setup.....	39
Figure 3.2 Spanwise averaged (left) and 2D contour of streamwise velocity (right)	40

Figure 3.3 y^+ contours of ribbed channel model	49
Figure 3.4 Mesh independency for Rke and YS models.....	50
Figure 3.5 Mesh structure at inter rib and turn regions.....	51
Figure 3.6 Mesh structure for smooth(top) and ribbed(bottom) cases	51
Figure 3.7 Convergence at monitor points	52
Figure 4.1 Smooth and ribbed channel Nusselt Number distribution (Re = 20000).....	54
Figure 4.2 Area Averaged Nu and Nu_{sm} results	55
Figure 4.3 Ribbed channel Nu/ Nu_{sm} distribution (Re = 20000, 35000, & 50000).....	57
Figure 4.4 Area averaged Nu/ Nu_{sm} Results (Re = 20000, 35000, & 50000).....	58
Figure 4.5 Spanwise averaged Nu along 4 th inter rib	60
Figure 4.6 4 th inter rib streamtraces for v2f (a) and low Re(b) (low) models and [59](c)..	60
Figure 4.7 Inter rib area averaged Nu results	61
Figure 4.8 Turbulence intensity check forYS model	62
Figure 4.9 Inter rib area averaged Nu_{sm} results	63
Figure 4.10 Nu and Nu_{sm} distributions for 3 turbulence models (Re=20000)	64
Figure 4.11 Stream traces at the bend region a)top view, b)front view, c)right view.....	65
Figure 4.12 Nu/ Nu_{sm} distributions and spanwise averaged results (Re=20000)	66

CHAPTER 1

INTRODUCTION

Gas turbines are typically needed by aircrafts and power plants to generate thrust or shaft power. Energy is extracted with open thermodynamic cycle similar to Brayton cycle through a rotary system (Figure 1.1). In an ideal gas turbine cycle, air is sucked into the turbine driven compressor and pressured isentropically and constant pressure combustion takes place in the combustor. Part of the energy drives the turbine by isentropic expansion and the rest of the energy stands as the useful power.

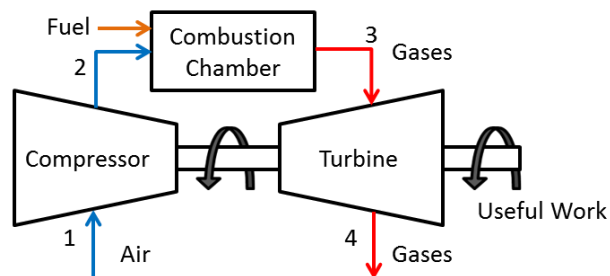


Figure 1.1 Open Gas Turbine Cycle

In order to increase the performance of the gas turbine, mass flow rate may be increased and/or higher temperature and pressure ratios at turbine and compressor stages can be introduced. However, that causes increase in size and weight of the engine. Regardless

of the mass flow, a parameter like specific work output is used [1]. Specific work output can be written as a function of the pressure ratio of compressor r , and relative turbine inlet temperature t as stated in Equations 1.1 and 1.2. Hence, higher pressure ratio of the compressor and higher turbine inlet temperature improves the work output from the cycle.

$$W = c_p(T_3 - T_4) - c_p(T_2 - T_1) \quad 1.1$$

$$\frac{W}{c_p T_1} = t \left(1 - \frac{1}{r^{\frac{\gamma-1}{\gamma}}} \right) - \left(r^{\frac{\gamma-1}{\gamma}} - 1 \right) \quad 1.2$$

The engineering focuses to design a successfully operating gas turbine are the efficiency, size, weight, emission and durability of the components. Temperature increase during the compression and combustion stages results in higher turbine inlet temperature T_3 . In modern aero engines, the turbine nozzle guide vanes and rotor blades are designed using temperature resistive materials with thermal barrier coatings. In addition, special cooling techniques are applied to meet the life requirements.

The need of high temperature applications is that the components must withstand the mechanical loads under the exposure of high temperature gas. Nickel based alloys are mostly used in gas turbine applications. They may be in the form of cast and wrought alloys. Their grain structure may be polycrystal (equiaxed and columnar) or single crystal [2, 3]. To improve the material capability to withstand the loads, several elements such as Ni, Cr, Co, Mo, W, Al, Ti etc. with various proportions are mixed inside the composition of high temperature alloys. Most of the power plant manufacturers have their own proprietary material for hot sections. Some of the developed materials are the variations of Inconel, Rene, Nimonic, Pyromet, Udimet etc. [2]. Table 1.1 shows some material development examples of different gas turbine manufacturers.

Table 1.1 Turbine blade materials [3]

Manufacturer	Model	Vanes	Blades	Coatings
ABB	11N2	IN939	IN738LC	NiCrAlY+Si
	GT24/26	DS CM247LC (R1)/ MarM247LC (R2,3)/ IN738 (R4,5)	DS CM247LC (R1-3)/ MarM247LC (R4,5)	TBC (R1V)/NiCrAlY+Si (R2-4 B,V) Uncoated R5V, Chromised (R5B)
GE	7/9EA	FSX-414 (all stages)	GTD-111/IN738/ Udimet 500	RT22/GT29-In+ (R1B)
	7/9FA	FSX-414 (R1)/ GTD-222 (R2,3)	DS GTD-111 (R1)/ GTD-111 (R2,3)	GT33-In/GT-29-In+/ Chromise (R3)
	7H	SC Rene N5 (R1)/ FSX-414/GTD-222	SC Rene N5 (R1)/ DS GTD-111 (R2,3)	TBC (R1,2 B,V)/ All others GT33
Siemens	V84/94.2	IN939	IN738LC/IN792 (R4)	CoNiCrAlY+Si
	V84/94.3A	SC PWA1483 (R1,2)/ IN939	SC PWA1483 (R1,2)	TBC (EB-PVD R1B)/MCrAlY+Re
Westinghouse/ Mitsubishi	501D5/701D	ECY-768/X-45	Udimet 520	MCrAlY
	501/701F	ECY-768/X-45	IN738LC	TBC (R1 B,V)/ MCrAlY/Sermalloy J
	501/701G	IN939	DS MarM002 (R1,2)/ CM247	TBC (R1,2 B,V)/ EB-PVD/MCrAlY

Note: R1, R2, etc. refer to the first, second rotor sections, etc.; B and V refer to blade and vane, respectively.

The gas temperatures are beyond the material limits in modern aero engine designs as depicted in Figure 1.2. This ability is achieved with the implementation of various cooling materials of hot section components.

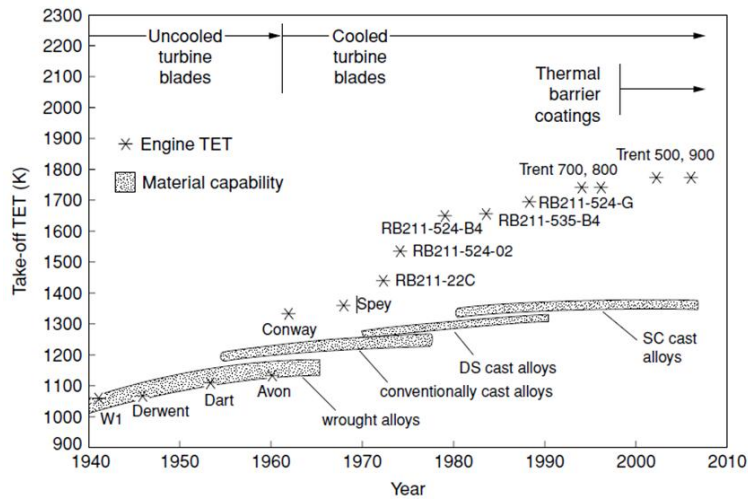


Figure 1.2 Evolution of the turbine entry temperature (TET) capability of Rolls-Royce's civil aeroengines, from 1940 to the present day [4]

Since the operating temperatures are already beyond the allowable material limits, turbine nozzle guide vanes and rotor blades are cooled with various cooling techniques so that they can withstand that working conditions. The aim is basically to protect the blades from reaching higher temperatures and thermal gradients. Blades are manufactured with small holes and internal cooling channels inside. Cold air is sucked from compressor rear stages and supplied through these channels and discharged into the main flow. At the secondary air path, the pressure drop of coolant air must be smaller than the one of the main flow at the combustion chamber in order to be able to discharge the coolant air from the turbine blades. Blades are cooled both externally and internally. Typical cooling applied rotor blade is shown in Figure 1.3.

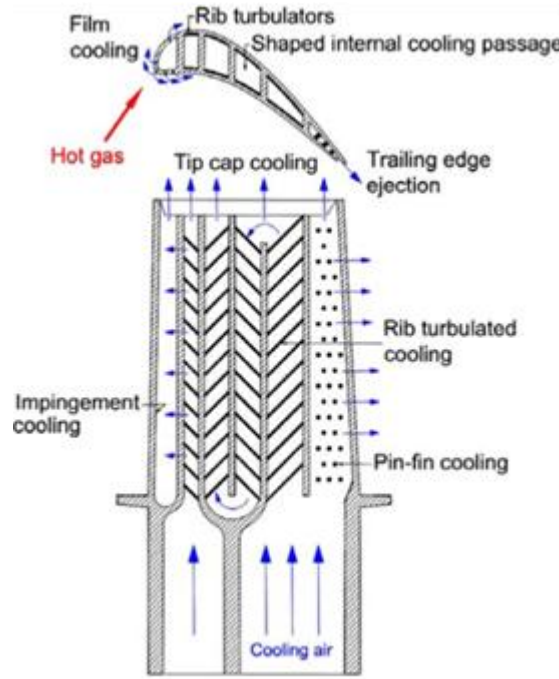


Figure 1.3 Cooling applied blade[5]

In external cooling (or film cooling), the cooling air is discharged through the holes and a protective film layer between the hot stream and blade material is obtained. Main part of the turbine blade cooling is achieved by film cooling. The main parameters that designers consider are the pressure ratio, temperature ratio, blowing ratio (mass flux ratio of coolant to main flow). Pressure ratio needs to be large enough for coolant to be discharged and low enough in order not to create a jet into the hot stream. Temperature ratio must be as low as possible to obtain desired heat transfer coefficients. Blowing ratio (mass flux ratio) is function of densities and velocities of coolant and mainstream and it affects the temperature profile of the mixture downstream the hole. Typically, pressure ratio, temperature ratio and blowing ratio are in the range of 1.02-1.10, 0.5-0.85 and 0.5-2.0, respectively [5]. The angle and position of the film cooling holes are other effecting parameters. To determine the cooled blade geometry, designers must also

consider the effects of unsteady wakes and free stream turbulence at the main stream on temperature distribution of the blades.

The internal flow and heat transfer characteristics of the turbine blades are highly dependent on the design of the cooling configuration. Maximum convective heat transfer through the internal surfaces is desired before the coolant is discharged from the film cooling holes and trailing edge holes. The pressure drop of coolant is critical and it should be minimized. The pressure ratio of the coolant and the main stream must be greater than unity in order to eject the coolant into the mainstream.

Convective heat transfer from the blade internal surface is achieved with impingement cooling and forced convective cooling in modern gas turbine blades. In most of the nozzle guide vanes and leading edge side of rotor blades, impingement cooling is applied. Jet coolant coming from neighbouring channel is impinged at the blade internal surface and convective heat transfer is achieved in impingement cooling. The mid chord and trailing edge regions of rotor blades are cooled with serpentine channel configurations due to the structural needs of blade. The channel cross-section and turbulence promoters like ribs, pins, fins, dimples and turns inside the channel are the geometrical effective parameters on pressure drop and heat transfer. Reynolds number inside the channel and the effects of rotation on the cooling performance is also considered. Serpentine channels enhance the convective heat transfer of the cooling channels. U or S-shaped serpentine channels with turbulence promoters are implemented inside the blades [5].

Present study aims to experimentally investigate the heat transfer inside a 2 pass square channel with ribs on one wall. Special attention is given to the effects of 180 deg circular turn and transverse ribs after the turn on heat transfer enhancement along the second pass.

1.1. Turbine Internal Cooling

Generally, the leading edge region of rotor blades are cooled by impingement cooling technique and trailing edge region is by pin fin cooling [5]. The rest of the blade is cooled by rib turbulated cooling because of the structural needs. In this section, main focus is given to the rib turbulated cooling techniques in literature.

Channels are generally designed for a mass flow rate and corresponding Reynolds number which is calculated based on hydraulic diameter. Channel aspect ratio or width to height ratio or channel shape, Reynolds number, channel blockage ratio, shape and placement of turbulators are the effective on the cooling channel performance [6]–[8].

It is necessary to define the geometrical parameters before interpreting the effects on channel heat transfer (Figure 1.4). In general, ribs are placed on two opposite surfaces of the cooling channels which correspond to suction and pressure side of the blade. Rib angle of attack is the angle between rib and the flow direction. Rib pitch is the distance from one rib to another. Channel blockage ratio is the ratio of the rib height to the channel height. In literature, the rib height to the channel hydraulic diameter ratio is also used to make comparisons of cooling performance.

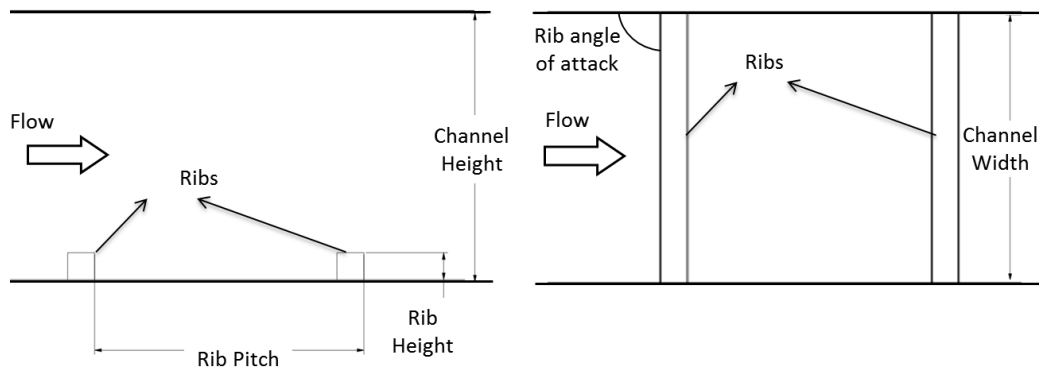


Figure 1.4 Channel with ribs on one wall, side view (left), top view (right)

1.1.1. Ribbed Channel Flow

The aim of the internal convective cooling is basically to increase the heat transfer inside the channel by understanding and improving the flow features to desired levels. In general, serpentine channel inside the gas turbine blades are roughened. However, depending on the heat transfer demand and temperature gradient problems related with the material structure, channels are partly roughened or remained smooth. The shape and amount of roughness elements should be considered to achieve desired heat transfer and pressure drop levels.

Ribs or turbulators enhance heat transfer by affecting the flow parameters of the cooling channel. Ribbs act like an obstacle for the flow and break the boundary layer creating secondary flows similar to forward and backward facing step. Periodic ribs break the laminar sublayer and create local wall turbulence because of separation and reattachment of flow between the ribs, that enhances the heat transfer on the surface [9]. Main incident that enhances the heat transfer is that flow reattaches the surface to recover the boundary layer creating a thin boundary layer. Detailed flow and heat transfer around the rib which is perpendicular to the flow is investigated experimentally [10]. The heat transfer distribution on the ribbed channel surface is determined with liquid crystal thermography and the flow field is investigated with PIV and oil visualization techniques. The rib induced secondary flows and pressure fluctuations at the rib vicinity are reported. Similar geometry with both 90 and 45 degree rib angles is investigated conducting LES analysis [11]. Secondary flow structures are tried to be detected and related to heat transfer using vortex detection methods.

There are numerous investigations offering correlations relating the heat transfer and pressure drop in literature. However, the designer must consider the limits of correlations and aware of flow characteristics and corresponding heat transfer behaviour of the cooling channels with different cooling configurations. All affecting parameters are investigated extensively in literature. Rib turbulated cooling is investigated in

numerous researches. The ones which are related with the current work is is mentioned in the introduction chapter.

Ribs spacing, rib angle of attack, rib cross section, rib height, channel cross section, rotation and U-bend geometry are the main effecting parameters that are explained regarding to the literature.

Rib Spacing: Ribs enhance heat transfer by breaking the heat transfer and letting it to be redeveloped. Rib spacing is an important parameter affecting the heat transfer area between two ribs. Rib pitch (P) to rib height (e) ratio has an optimum value in terms of heat transfer which varies depending on the other parameters like channel rib shape and rib angle etc. Typically the heat transfer enhancement factor gets close to unity when it is too small or too large. Han et al. [12] studied the rib spacing effect experimentally with sharp edged ribs and 0.056 rib height to hydraulic diameter ratio. They reported that flow cannot reattach to the surface with ribs with small distance, which are having P/e less than 5. For larger rib pitch to rib height ratios, maximum heat transfer and maximum pressure drop is obtained with P/e of 10. For larger rib pitch to rib height ratios, heat transfer and frictional losses decrease gradually due to redevelopment of boundary layer. Liu²⁷ [13] conducted experiments at both stationary and rotating condition with various Reynolds numbers and P/e ratios from 3 to 10 with channel having aspect ratio of 1:2. The aspect ratio of the channel was 0.5. For stationary cases, it was reported that highest heat transfer is obtained at P/e=5. Depending on the Reynolds number, highest thermal performance is observed at P/e from 5 to 7.5 regarding both heat transfer and pressure drop. Ahn et al. [14] investigated the channel model with square and semi circular ribs both numerically and experimentally. Turbulence intensity around the ribs and local velocity contours are determined by LES and the relation with local heat transfer results are discussed. It is found that the total heat transfer including the one on ribs values are similar and the pressure drop is lower in channel with rounded ribbed case when compared to the one with square ribs.

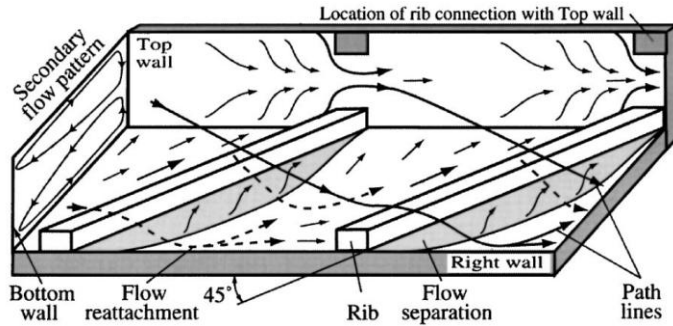


Figure 1.5 Secondary flows due to 45deg ribs[15]

Rib Angle of Attack: Creating an obstacle to the flow mostly enhances heat transfer inside a channel. The attack angle of the obstacles or ribs creates secondary flow structures inside the channel [16]. The mixing inside the channel depends on that vortical structures created by ribs. Several rib shapes with corresponding vortical structures are depicted in Figure 1.5. Çakan [10] conducted experiments on square channel with 30, 45, 60 and 90 deg rib angles and reported that channel with 45 deg ribs show better performance in terms of the heat transfer. Kiml et al. [15] conducted flow visualization and thermocouple measurement studies on channel with 2 aspect ratios having 90 deg, 75 deg, 60 deg and 45 deg ribs. It is found that angled ribs create secondary flows and cause flow to impinge rib trailing side smooth wall increasing heat transfer rate. Maximum heat transfer and friction factor is achieved at 45 deg rib case. Park et al. [8] studied the channels experimentally with varying aspect ratio and rib angles and showed that specific rib angles are appropriate for different aspect ratios, but mostly channels with 45-60 degree ribs performs better regarding heat transfer and pressure drop. In addition, angled ribs generally creates relatively larger heat transfer rates with lower pressure drop at channels with narrow aspect ratios, on the other hand transverse or 90deg ribs perform better at channels with aspect ratios larger than one [8]. Channel with V-shaped ribs with 45 and 60deg V angle is investigated experimentally by Kukreja et al. [17]. It is stated that channel with 60deg V-shaped ribs generates the highest heat transfer enhancement. Vass [11] conducted simulations (LES) to compare

the flow and coherent structures and showed their relations to heat transfer at the heated surface for the cases with 45 and 90deg ribs.

Rib Cross-section and rib height: It is necessary to assess the effects of rib cross section because the ribs are responsible for the size of the secondary flows at the rib vicinity. Different rib shapes and profiles are depicted in Figure 1.6.

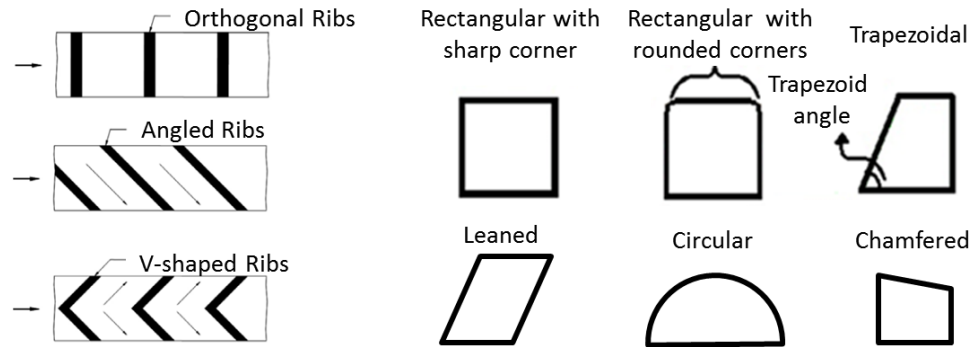


Figure 1.6 Rib shape and rib cross-section examples

Blades are manufactured with casting most of the time, therefore ribs with sharp edges cannot be manufactured perfectly. As a result, the effects of rib profile and rib height (or blockage ratio) are needed to be clarified. Blockage ratio is defined as the ratio of rib height to channel height. Han [18] investigated the effect of rib height on the ribbed and smooth wall heat transfer with ribs with 90deg rib angles. It was concluded that the heat transfer for both ribbed and smooth surfaces increased but the enhancement on smooth wall was more sensitive to rib height. Rib height to hydraulic diameter ratio was varied between 0.021 to 0.063. Rallabandi et al. experimentally studied the effects of both rib height to hydraulic diameter ratio and rib pitch to rib height ratio with angled ribs with filleted cross section. Rib heights were from 0.094 to 0.188 and it is found that increasing rib height does not increase the heat transfer enhancement significantly when pressure loss penalty is considered. Rib height effect was more effective than the rib spacing effect regarding the pressure loss. Taslim et al. conducted experiments with

varying rib cross sections [19]. They found that ribs with higher height/width ratio creates higher heat transfer and pressure loss. In addition, ribs having high height/width ratio in trapezoidal shape drops the pressure loss with same heat transfer level. Thermal performance of a channel with ribs and grooves was investigated experimentally for one wall heated and fully developed flow condition by Layek et al. [20]. Ribs were chamfered from the top surface and different chamfer angles ranging from 5 to 30 degrees are investigated. It was reported that maximum Nusselt number was found at chamfer angle of 18 deg and pressure drop increased with increasing chamfer angle. Effect of rib lean as a cooling performance parameter is investigated experimentally by Bunker et al. [21]. Ribs are leaned towards both upstream and downstream with angles of 22.5 deg and 45 deg. The results show that the lean application drops the heat transfer and increases the friction in cooling channels. Rallabandi et al. [22] investigated and proposed correlations regarding the effects of round edge angled ribs, rib spacing and rib height, experimentally. The pitch/rib height ratio is taken from 5 to 10 and rib height/channel diameter varied from 0.095 to 0.19. It was found that larger rib spacing provides better cooling performance for the channels with both rounded and sharp ribbed cases. The friction factor of rounded ribbed case is lower than the one with sharp edged ribbes especially at high blockage ratios or rib height to hydraulic diameter ratios. The reason of that drop is reported as it is due to the smaller recirculation zones at the rib vicinity. Kamali et al. [23] numerically investigated the effect of rib profile with square, triangle and trapezoid with decreasing/increasing height in flow direction ribs for a square channel with ribs on one wall. The blockage ratio was 0.1, Reynolds number was varied from 8000 to 20000 and P/e ratio was varied from 8 to 15. They validated the SST k- ω model with the experimental data of Wang et al. [24]. According to the results, the channel equipped with trapezoidal ribs with increasing height in flow direction provides the highest heat transfer enhancement and the one equipped with trapezoidal ribs with decreasing height in flow direction provides the lowest heat transfer enhancement.

Channel Cross-section: The serpentine channels with various aspect ratios are applied regarding the turbine blade aerodynamic and structural design. Han et al. and Park et al. conducted experimental analysis on channels with aspect ratios from 0.25 to 4 with different rib angles of attack. It is stated that angled ribs are more effective on low aspect ratio channels in terms of heat transfer and pressure drop [7, 8], in other words the positive effect of secondary flows on heat transfer fade away as aspect ratio increases [6]. In addition, transverse ribs perform better at square channels for a fixed friction factor. Agarwal performed experimental investigation using naphthalene sublimation technique on 2 pass channel with aspect ratios of 0.25 and 4. It is reported that channels with wider cross section or high aspect ratio provide higher heat transfer rates because of the wider rib turbulator surface [25]. Kiml et al. [26] performed flow visualization and numerical simulation study with a high aspect ratio trapezoidal channel model similar to turbine blade trailing edge cooling passage. They focused on the secondary flow structures and showed that the trapezoidal effect causes uneven flow distributing allow more mass flow rate to the wider side and the rotational momentum of secondary flows increase with rib inclination.

Effect of Rotation: The flow inside a rotating channel is significantly different from the flow inside a stationary channel. In general, experimental and numerical investigations of cooling channels are conducted for stationary and rotating conditions. Lezius et al. [27] investigated the effects of rotation on the flow in a rectangular channel. They reported that the instability characteristics on the leading wall (corresponds to suction side of a rotating turbine blade) are different from the trailing wall. The nomenclature of the rotating blade is depicted in Figure 1.7.

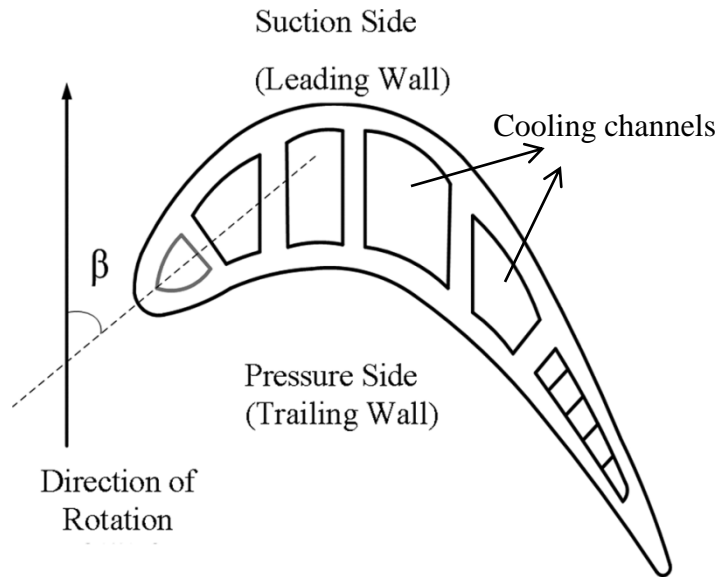


Figure 1.7 Rotating blade and internal channels

The flow and heat transfer features of cooling channels are influenced by the Coriolis and buoyancy forces under the effect of rotation. The radially outward flow is affected unlikely to the radially inward flow. In radially outward case, flow penetrates to the trailing wall, which corresponds to pressure side of the rotor blade, and increases the instability and heat transfer, besides the heat transfer at the leading wall decreases. In radially inward flow case, rotation destabilizes the leading wall boundary layer and increases heat transfer rate. Wagner et al. [28] experimentally investigated the effects of buoyancy and coriolis forces on rotating serpentine rectangular channel. For the radially inward flow, it is reported that the heat transfer relative to the non-rotating case is larger on the leading surfaces and smaller on trailing surfaces. In radially outward flow, the increase in heat transfer is larger than the radially inward ones. Wagner et al. [29] also experimentally investigated the effects of rotation on ribbed serpentine channels. The ribs are placed perpendicular to the flow direction. The change in heat transfer enhancement due to rotation is found as it varies by a factor of four and rotation has more significant effect on ribbed case heat transfer than smooth case. The results also

showed that the maximum increase in heat transfer of the rotating ribbed case is only slightly larger than the rotating smooth wall case. It was concluded that the effects of Coriolis and buoyancy forces must be considered in cooling channel design.

Multipass channels: Depending on the design of cooling channels, cooling configurations often include serpentine passages. The effects of turn regions on flow and heat transfer features are needed to be investigated. Characterization of flow inside smooth curved channels with square and circular cross section are studied experimentally in the literature [30]–[32]. Dean type secondary flow structures develop due to the bend section influencing the flow field and heat transfer characteristics of downstream channel. Depending on the geometry of the bend, flow separates and reattaches the inner side wall at downstream channel. Wang et al. [33] conducted numerical analysis to determine the effect of U turn geometry. The heat transfer results agreed with the experimental case of Chyu [34] for the sharp turn case. They stated that a sharp turn rather than circular one creates more strong swirl after the turn. Saha et al. conducted RANS simulations to investigate the effect of turn shape on flow and heat transfer inside a two pass channel [35]. Addition of turning vane and periodic dimples and geometry variations on inner and outer walls at the turn region were the effecting parameters. 9 different U-bend geometries investigated for minimizing the pressure loss and maximizing the heat transfer. The results show that dimples at the U-bend section don't effect the secondary flows at the U-bend significantly, enhances the heat transfer moderately. Implementation of turning vane decreases both pressure loss and heat transfer and symmetrical bulb shaped thin inner wall performs better in terms of heat transfer and pressure loss. Hirota et al. [36] experimentally investigated the effect of inner wall clearance on the heat transfer inside a two pass channel with 180 deg sharp turn using naphthalene sublimation technique. They concluded that there is a steep change in the detailed maps of heat transfer rates of the second pass outer wall depending on the clearance. Serpentine ribbed channels are widely investigated in order to improve the

performance of cooling passages. Chen, et al. [37] investigated heat transfer and pressure drop in 2-pass channel with different turning vanes. Experiments using liquid crystal thermography and numerical analyses using RANS models (ORS, SST, k- ϵ) are compared. It is stated that Omega Reynolds Stress Model (ORS) model performs better and configuration with turning vane creates less pressure loss and heat transfer compared to baseline. Combined effect of ribs and the turn geometry is addressed only in a few study. Secondary flows due to rib angle affect the flow development through the turn region in multipass channels. Mochizuki et al. [38] experimentally investigated a two pass ribbed channel with 180 deg. sharp turn. The rib height to hydraulic diameter ratio was 0.09 and rib angles were 30, 45, 60, 75, 90 deg. The results show that different rib arrangements create considerable differences in cooling performances of the entire channel. In the study, channel is equipped with ribs on both passages or one of them is remained smooth, it was concluded that applying the same rib configuration changes the pressure drop depending on the pass it is applied. The numerical simulation of the experimental geometry under stationary and rotating condition were performed with smooth and ribbed cases [39], [40]. Large eddy simulations showed that the heat transfer at the turn region and second pass increased due to the flow impingement and the turn induced secondary flows at the stationary case and it was stated that the pressure drop is much more sensitive to rib arrangements and rotation than the heat transfer. Heat transfer at the outer surface of the turn region is of interest in terms of tip cooling performance of the turbine blade. Wang et al. [41] conducted experiments using liquid crystal thermography with one smooth (reference) and seven different rib-roughened surfaces on outer wall. The Reynolds numbers were 20000 and 26000 based on hydraulic diameter. According to the results, it is indicated that the local heat transfer enhancement was dominated by the impingement of the flow for the smooth case and ribbed configurations augments heat transfer rates with a penalty of non-uniform heat transfer distribution. Ribs at outer wall configurations cause a much larger pressure drop

at the turn section and, 45 deg V-shaped ribs performs the best in terms of thermal performance.

1.2. Motivation

2-pass channel with square cross section will be used for internal cooling performance tests at Reynolds numbers of 20000, 35000, and 50000. Reynolds number is calculated based on the channel hydraulic diameter. The numerical simulations are compared with experimental data. Flow investigation to understand the flow-heat transfer relation downstream of the turn section is performed. The channel geometry is fixed to specific cooling channel parameters of 10 for rib pitch to rib height ratio, 10 % for rib blockage ratio (0.1 for rib height to hydraulic diameter ratio). Square rib cross-section and circular rounded inner and outer U-bend shapes are chosen for experimental setup and the results are compared with the numerical simulations. On the bottom wall of the channel, ribs with square cross section are placed perpendicular or orthogonal to the flow direction meaning that the rib angle of attack is 90. It is advantageous to perform detailed numerical analysis with these geometrical parameters because there are plenty of experimental and numerical studies regarding these geometrical parameters. The details are stated at the experimental procedure section.

CHAPTER 2

EXPERIMENTAL PROCEDURE

2.1. Design of the Experimental Setup

Geometric Similarity in Cooling Ducts: In order to relate the heat transfer and flow inside the cooling ducts, the variables related to heat transfer and flow must be specified. Convective heat transfer in cooling ducts is dependent on the parameters such as temperature difference ΔT between the wall of the channel and the flowing fluid, channel hydraulic diameter D_h , mean velocity U_m , bulk temperature of the fluid and the material properties of the fluid like c_p , ρ , μ and k . For cooling ducts, Buckingham's π theorem results in an expression relating the Nusselt number to four main parameters which are shown in Eqn. 2.1 [10].

$$Nu = f\left(Re, Pr, \frac{T_m}{\Delta T}, Ec\right) \quad 2.1$$

$$Ec = \frac{U_m^2}{c_p \Delta T} \quad 2.2$$

Regarding the $\frac{T_m}{\Delta T}$ term relating the temperature, the variation in physical properties of the fluid is not significant and the temperature ratio is small, therefore the third term of the expression is usually omitted. That approach is experimentally validated by Kay & Nedderman [42].

Ec is the Eckert number (Eqn. 2.2) which represents the relative importance of the dynamic temperature and the temperature difference. That dimensionless term is considered in high speed compressible flows where viscous energy dissipation is needed to be significant. Since the flow inside the channel has low speed and is incompressible, the fourth term is omitted. Eqn. 2.1 becomes:

$$Nu = f(Re, Pr) \quad 2.3$$

Prandtl numbers are very close and around 0.7 for the experimental model and a real cooling channel of a gas turbine blade. Reynolds numbers are matched for experimental and real case in order to complete the Nusselt number similarity.

Inlet Section: In order to provide a fully developed turbulent flow to the test section, a straight entrance with same cross-section is provided. The length of the entrance is approximately 28 times channel hydraulic diameter which is larger than the hydrodynamic entry length for turbulent flow, [42, 43]. A flow straightener honeycomb is provided at the entrance. Channel hydraulic diameter to honeycomb cell inner diameter ratio is 25 and honeycomb thickness to cell size ratio is 6.25.

Settling Chamber: The flow enters inside the settling chamber after passing through the test section. The hydraulic diameter of test channel is 80 mm and the hydraulic diameter of the settling chamber is about 1000 mm. This provides a large area ratio decelerating the flow velocity 156 times. The mean velocities inside the channel are about 3.92, 6.86, 9.80 for Reynolds numbers of 20000, 35000 & 50000, respectively. That corresponds to a maximum velocity of 0.063 m/s for the $Re=50000$ case inside the settling chamber and it is assumed to be stationary.

Geometric Description of The Experimental Model: Experimental setup for internal cooling model tests is an open circuit wind tunnel with a two pass test section. Air is sucked at the inlet and it develops through the entrance section, respectively. Test section covers the heated test section and pressure measurements planes. Downstream of

the test section, air is discharged through the settling chamber and the fan, respectively (Figure 2.1 & Figure 2.2).

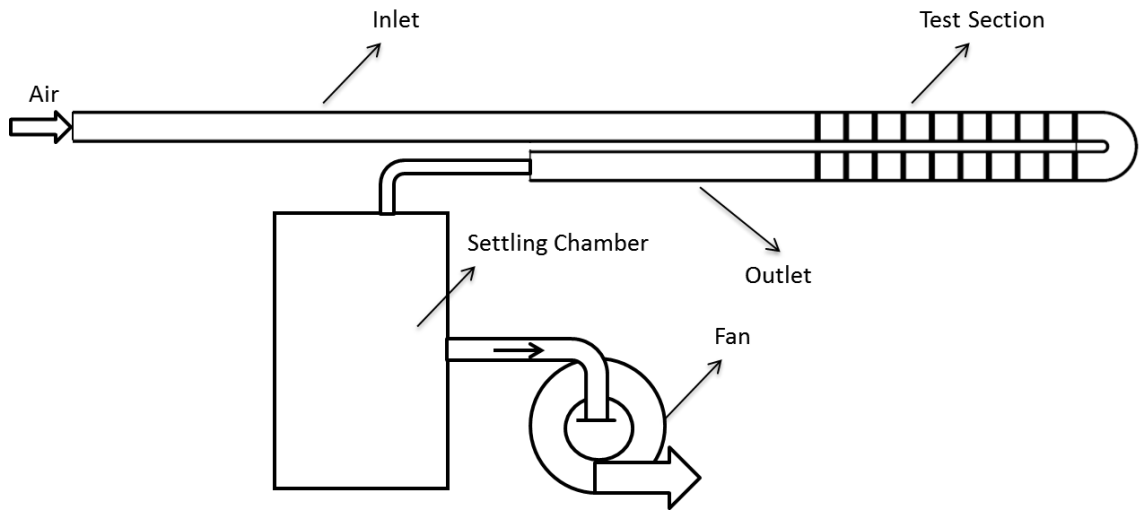


Figure 2.1 Experimental setup

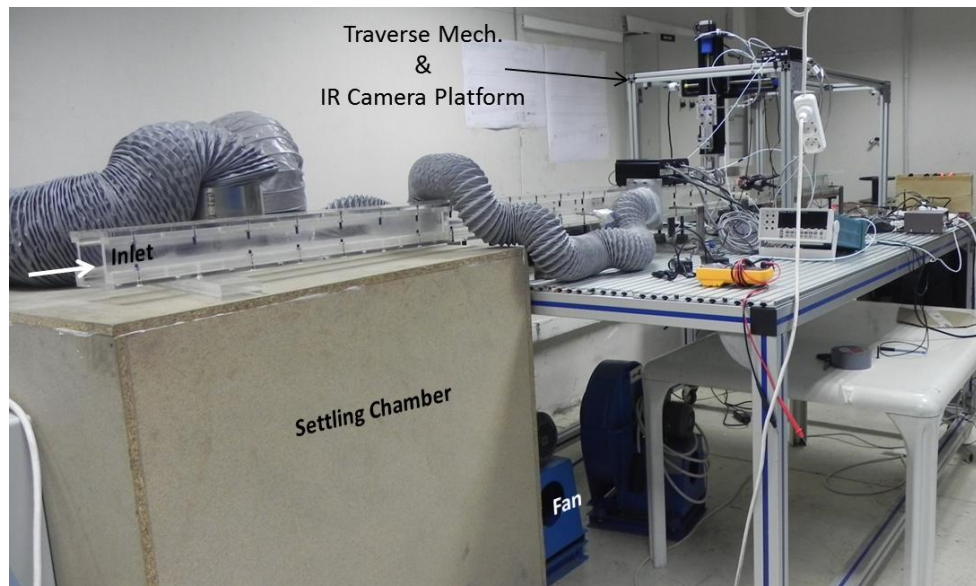


Figure 2.2 Experimental facility

The heated test section of the experimental channel model consists of three main parts which are two straight parts and a U turn section. Detailed drawings are depicted in Figure 2.3, Figure 2.4 & Figure 2.5. The scale factor between the tunnel and a real turbine blade channel is about 20 with equivalent Reynolds number. In order to get the desired uncertainty levels for pressure and temperature measurements, 80×80 mm square cross-section is decided which corresponds to 80 mm hydraulic diameter (D_h). This is important in surface temperature resolution in infrared measurements. For the present case, 3×3 pixels area covers a surface having 1 mm^2 area and there are 25 pixels through 1 rib height.

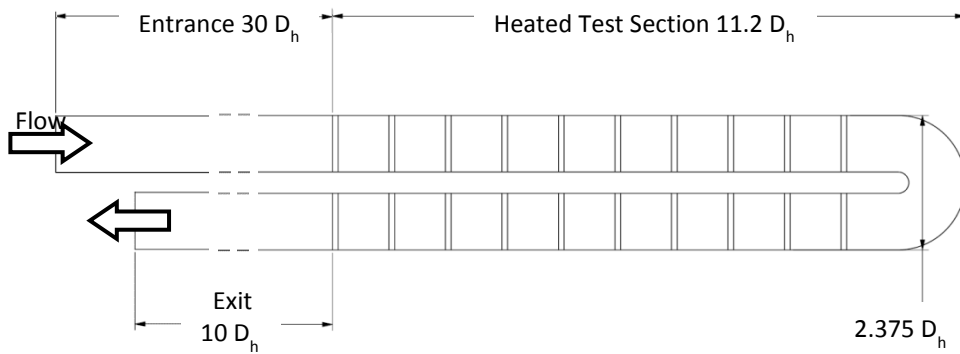


Figure 2.3 Tunnel description (top view)

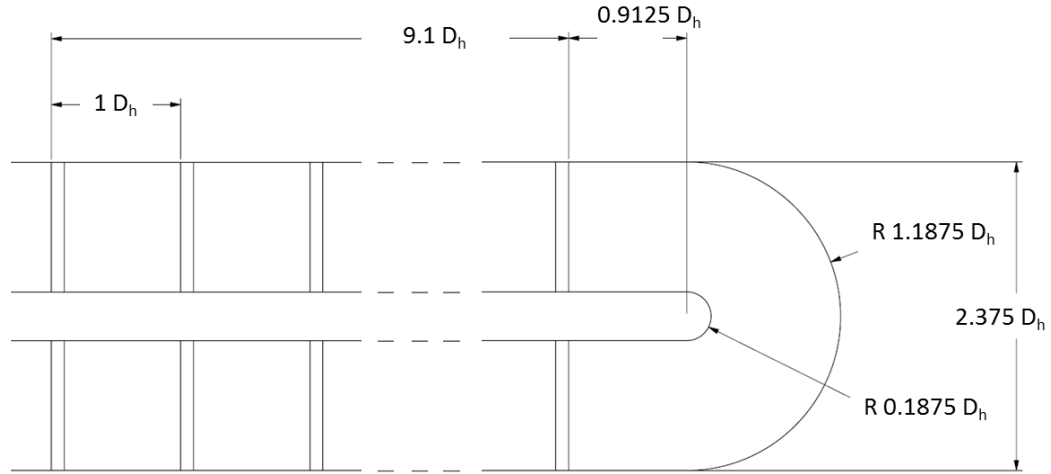


Figure 2.4 Test section

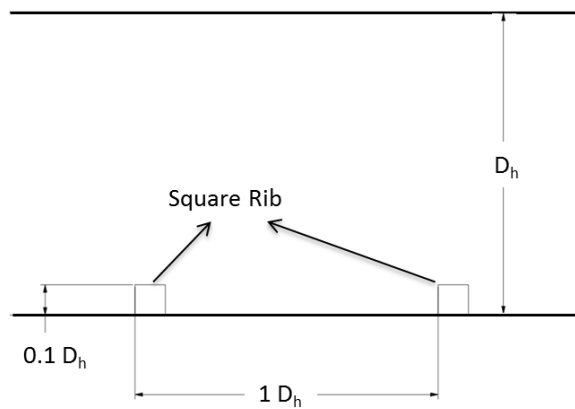


Figure 2.5 Rib geometry (side view)

The walls of the tunnel are machined from plexiglass, which has low conductivity ($k_p = 19 \text{ W/mK}$) so the heat conduction is assumed to be 1 dimensional. Plexiglass material is easy to machine and transparent for potential flow visualization studies.

Rib turbulators are placed only on the bottom wall of the heated test section. The angle between ribs and flow direction is 90 degree and the ribs have square cross-section. To verify the development and periodicity of the heat transfer at heated ribbed wall, 10 ribs

are provided before and after U-bend. Between two straight sections a 180 degree bend is provided to simulate the turn inside the blade.

2.2. Instrumentation and Measurement Techniques

The measurements are planned to be conducted at certain sectors. For pressure and air temperature measurements before and after heated test section, 2 sectors are defined. At the heated test section, temperature measurements are conducted at 19 sectors. Measurement locations are shown in Figure 2.6. Temperature sectors are the surfaces between the consecutive ribs where infrared temperature measurements are taken. Extra thermocouple measurements are taken at outside center of each temperature sector in order to get the heat loss from bottom wall (see Figure 2.11). Pressure sectors are defined before and after the heated test section. Total and static pressure measurements are conducted at two planes perpendicular to the flow direction. Air temperature probe is attached to the pressure pitot probe.

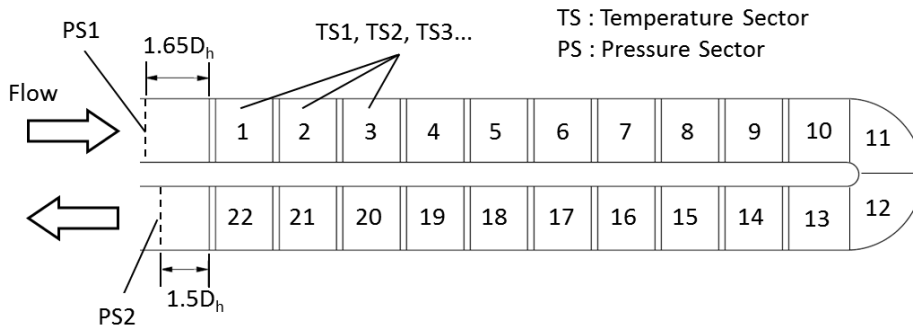


Figure 2.6 Measurement Sectors of Test section

2.2.1. Air Velocity and Temperature Measurements

Air temperature is determined using thermocouple measurements at the pressure sectors. Air temperature along the channel is assumed as stepwise or it increases at a constant rate and it is taken as constant along each inter rib space. Figure 2.7 shows the stepwise approximation of air bulk temperature inside the heated channel.

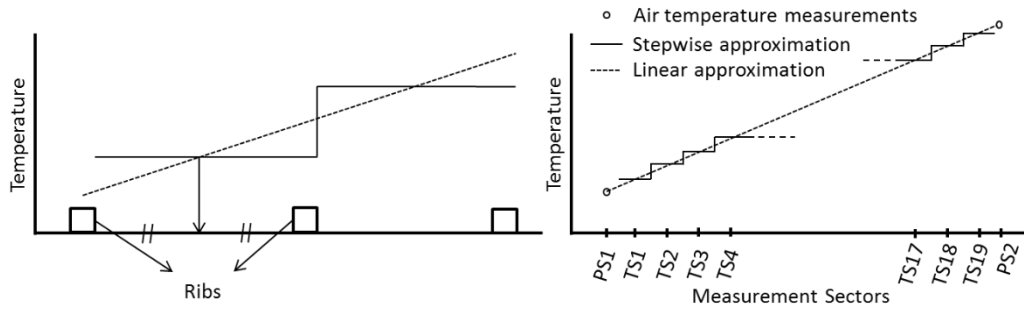


Figure 2.7 Air temperature estimation along the channel model

The measurement locations shown with relevant dimensions are depicted in Figure 2.6. The inlet station is equipped with reference probe which contains a thermocouple and pitot probe. T-type thermocouples with junction diameters of $250\ \mu\text{m}$ are selected for gas temperature measurements, which offer good accuracy and high time response. Picture of air flow probes is shown in Figure 2.8.

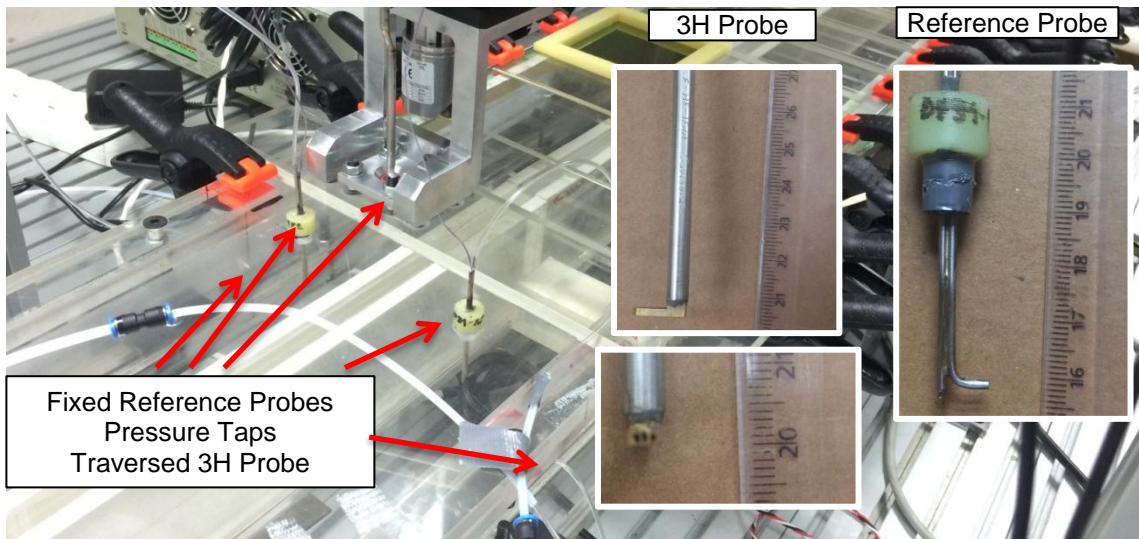


Figure 2.8 Flow measurement probes

Pitot probe is located 62% of the channel height whereas thermocouple measures the inlet gas temperature at 59% of the channel height. The probe is located to the center in

spanwise direction. The second reference probe with similar characteristics is also located at the outlet of the tunnel. The static pressure is measured by using wall static taps located only on the outer wall at mid-channel height and they are aligned with the reference probe heads for both inlet and outlet. Both of the reference probes are used to set the flow conditions for each experiment. Additionally, the pressure variations are also recorded during experiments in order to make sure the tunnel always operates with the adjusted flow conditions.

The ranges of the sensors are 25, 62 and 125 Pascals for three Reynolds numbers, and they have accuracy of 0.5% of full span. Pressure and T-type thermocouple measurements are taken with a sampling rate of 15 Hertz for one minute. At each inter rib space, infrared image is taken with a sampling rate of 25 Hertz. For the calculations, average pressure, thermocouple, and infrared image data are calculated.

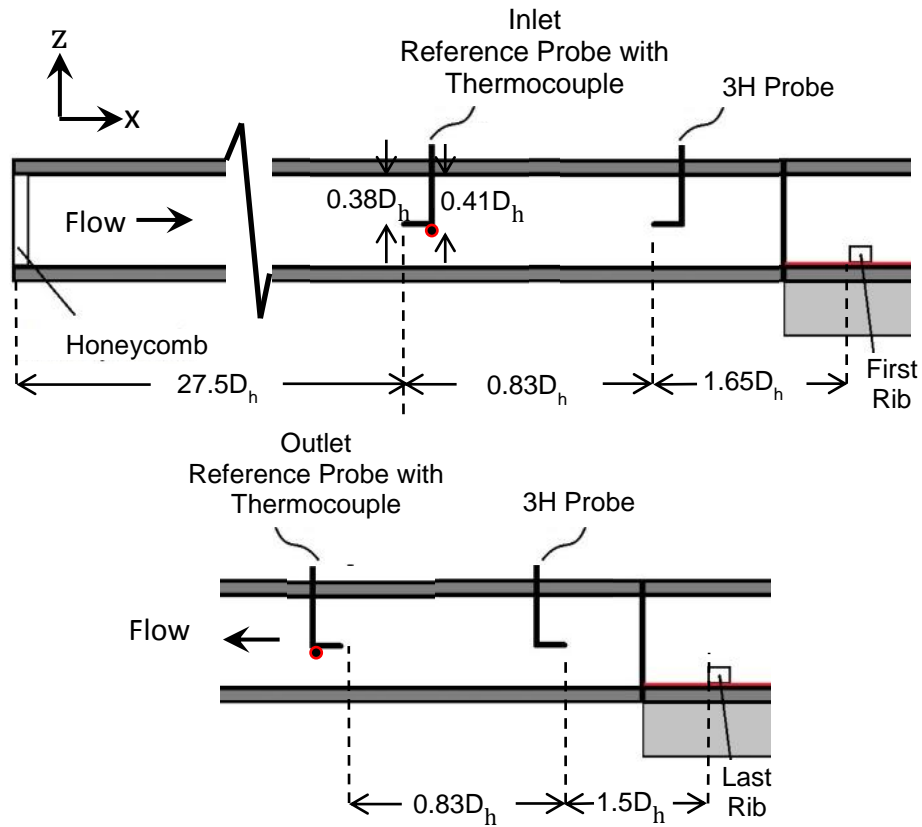


Figure 2.9 Probe instrumentation at inlet(upper) and outlet(lower)(not to scale)

A traversing mechanism is installed to the test section which allows characterization of flow field in both spanwise (along rib span) and vertical directions. The probe is moved in both directions by stepping motors which are controlled by a computer. The bilinear traversing mechanism produces a linear movement of 1 mm/rev. having a rate of 2.5 mm/s. Two encoders are mounted to the traversing unit in order to trace the amount of movement during experiments. The encoders produce 1000 pulses per rotation.

2.2.2. Heating the model

Foil heater technique is applied to obtain the heating condition. The heated test section part is heated from the bottom wall. Voltage is applied from two ends of the inconel

sheet and constant heat flux (approximately 400 W/m^2) boundary condition is provided from the bottom wall (Figure 2.10 & Figure 2.11).

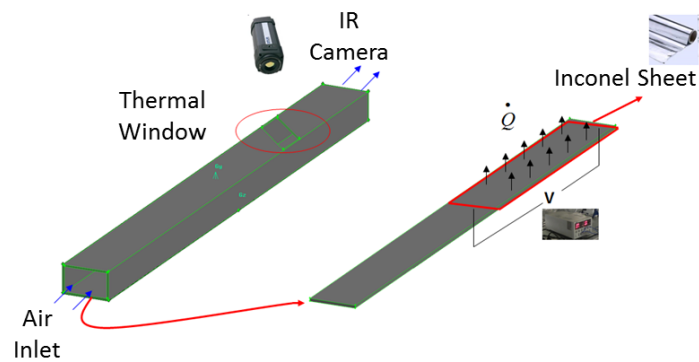


Figure 2.10 Tunnel heating

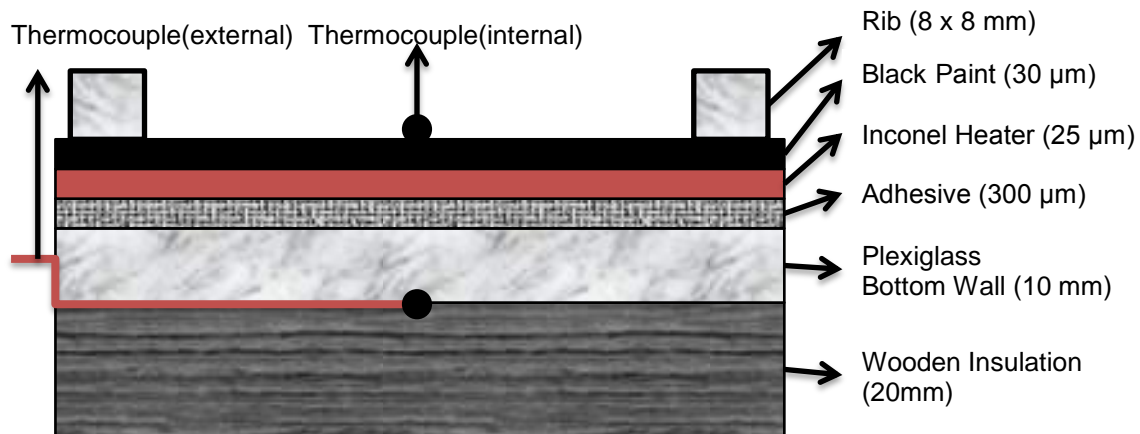


Figure 2.11 Inconel foil heating composite (not to scale)

A try and error strategy is attempted to decide how to heat a two pass channel with a circular U-bend. For the specific case, two different approach is tested with a smaller plate. The pictures and the temperature maps of two cases are shown in Figure 2.12. In

both cases, changing the span of the heater does not provide a constant temperature distribution.

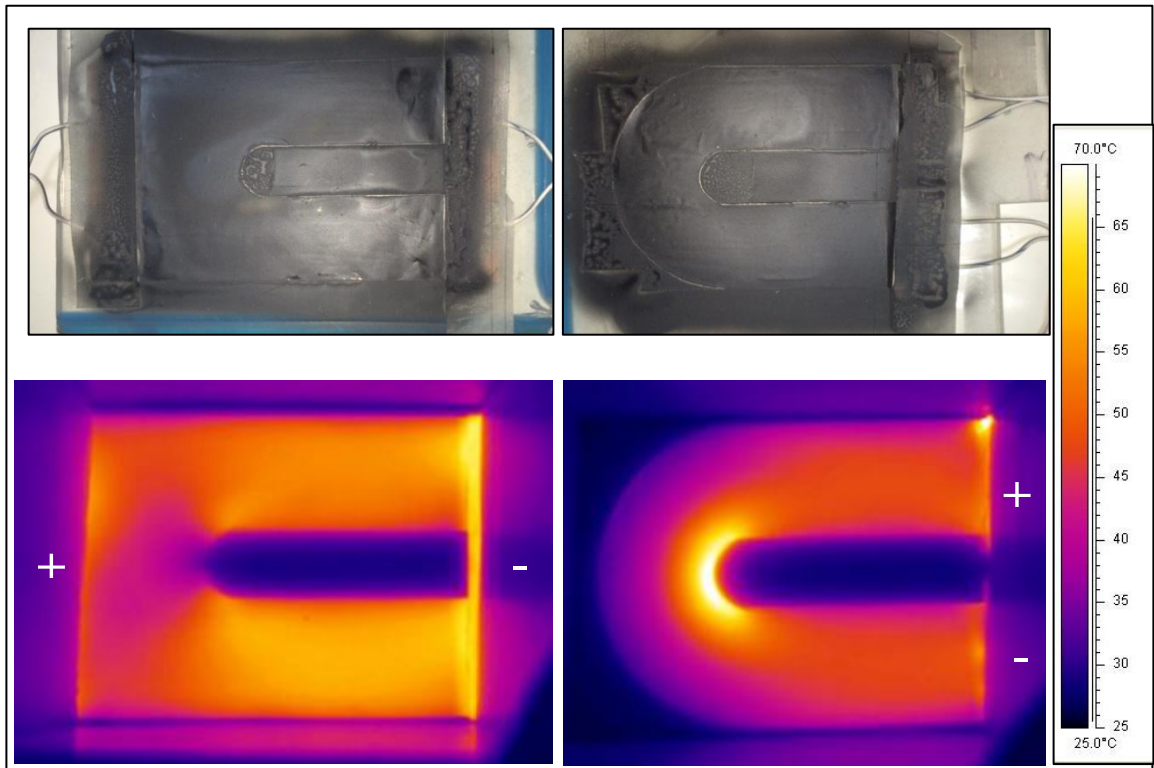


Figure 2.12 Photos(top) and temperature contours(bottom) of the heater decision study

As a consequence, both 1st and 2nd channel is heated with a one-piece heater involving the divider wall. Therefore, the bottom of the bottom wall is also heated at the tests.

2.2.3. Temperature Measurements

Temperature sectors 7 and 8 are instrumented with thermocouples. Six T-type fine-bare thermocouples are glued on the surface between two ribs as depicted in Figure 2.13. The junction diameter of the thermocouple is selected as 50 μm , which corresponds to 0.625% of rib height, in order to create minimum disturbance to the flow field. The thermocouple measurements are used to verify the IR camera results. The difference between the internal surface thermocouples and the corresponding infrared data is

measured to be less 0.25K. Therefore, there is no need to include an infrared data correction. Additionally, three thermocouples with junction diameters of 250 μm are located below the bottom wall (outside of the tunnel). Those thermocouples are used to compute the heat loss to the ambient. Hence, the net heat flux to the test section is calculated by subtracting the heat loss from heater power.

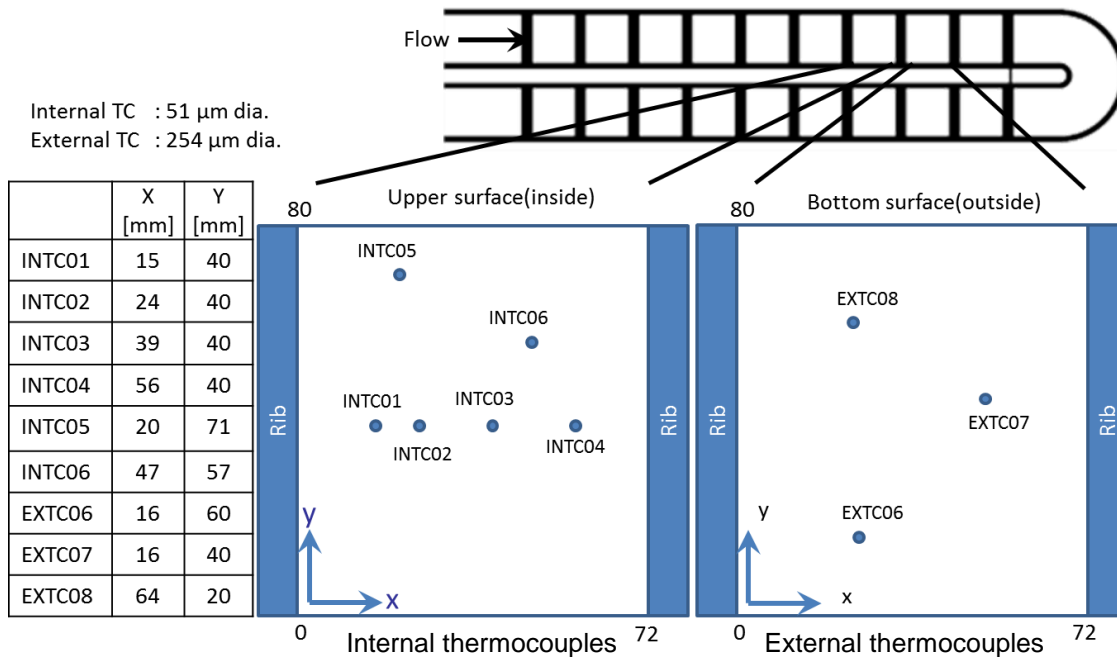


Figure 2.13 Internal (left) and external (right) thermocouple locations

In order to determine the temperature of heated wall, infrared thermography is used. BBAR coated germanium window is placed at the upper wall of the cooling channel model for each temperature sector. Infrared transition of the window is applicable for the specific measurements that the temperature values are expected to be changing from 25° to 70° C (Figure 2.15).

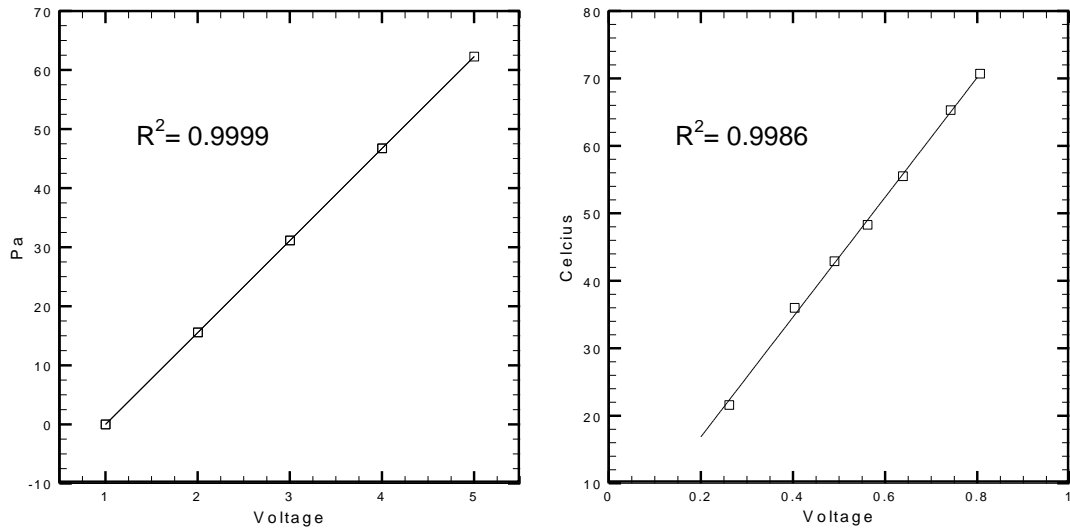


Figure 2.14 Temperature and pressure calibration examples

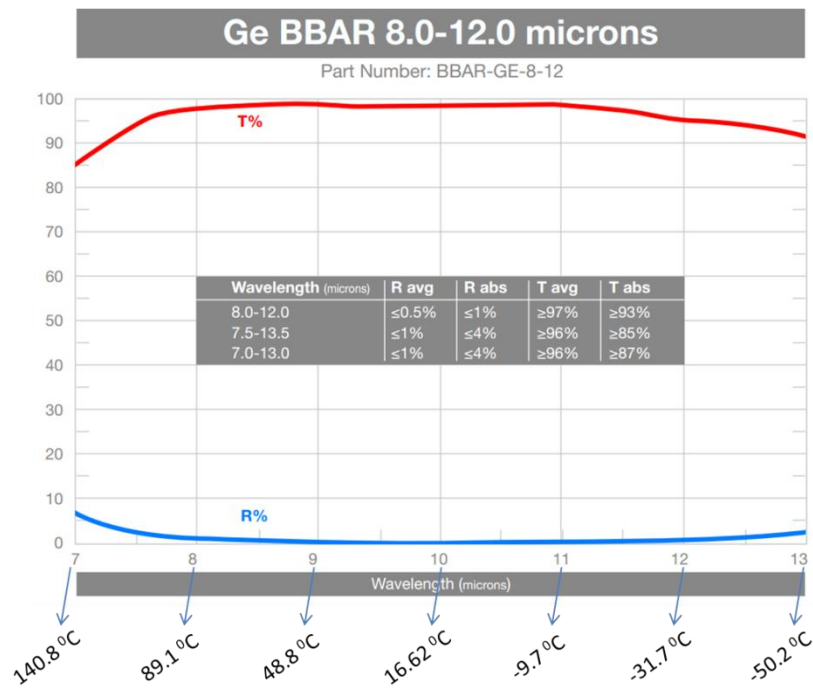


Figure 2.15 Transmissivity of the infrared window

2.2.4. Test Procedures

Data Reduction

Heat flux applied to the inconel foil was determined using eqn 2.4. The voltage across the inconel foil is measured using a multimeter. Voltage V across the inconel does not change in lateral direction. Current I across the inconel is determined simply by DC power supply.

$$q = VI \quad 2.4$$

Losses are determined with eqn. 2.5 using 1-D conduction assumption across plexiglass. Local temperature just above the thermocouple location is used to determine the losses and loss heat flux q_{loss} is assumed to be the same for the whole heated area.

$$q_{loss} = k_{pl}(T_w - T_{tc}) \quad 2.5$$

Local heat transfer coefficient is calculated between two rib turbulator using the thermal information.

$$h = (q - q_{loss})/[A(T_w - T_g)] \quad 2.6$$

The local Nusselt Number is calculated using the hydraulic diameter of channel and air thermal conductivity corresponding to bulk temperature (eqn. 2.7) . Nusselt number is normalized using the smooth wall measurement results.

$$Nu = hD_h/k_{air} \quad 2.7$$

Experimental Steps

In this part, how to obtain the row data will be explained in the order of data reduction and will be briefly mentioned. In equation (3.1):

V - voltage across the inconel foil is obtained applying the multimeter at both ends of the heated section as shown in Figure 2.10. I - current is simply taken from the DC power supply.

k_{pl} is the thermal conductivity of plexiglass material is taken as 0.19 W/mK, [45], [46].

T_w is the local temperature of the heated surface is obtained using the thermal camera data. Thermal camera value is taken using the “ThermaCam” software of the infrared measurement product. T_{tc} is the temperature measured by loss thermocouples and A is the heated area for the inconel foil. T_g is the bulk temperature for air.

D_h is the hydraulic diameter of the channel which is calculated by eqn. 2.8 and k_{air} is the thermal conductivity of air is determined using the properties of air at atmospheric pressure.

$$D_h = \frac{4WH}{P} \quad 2.8$$

Re is Reynolds number is determined using the bulk velocity which is obtained by the differential pressure measurements. Velocity is obtained from the difference between total and static pressure as shown in eqn 2.9.

$$u = \sqrt{\frac{2\Delta p}{\rho_{air}}} \quad 2.9$$

Pr is Prandtl Number which is taken as 0.69 using eqn. 2.9.

$$Pr = \frac{c_p \mu}{k} \quad 2.10$$

Post Processing Algorithm

Post processing of the experimental data is done by Matlab and Tecplot softwares. The post processing algorithm is presented in Figure 2.16. Part A is for determination of net heat flux. Heat flux data is calculated by Joule heating formula 2.4. In part B, infrared image is processed and used for heat transfer coefficient and Nusselt number calculation 2.7. Same procedure is followed for both smooth and ribbed configurations. Heat

transfer enhancement factor is obtained dividing ribbed channel results by smooth channel results.

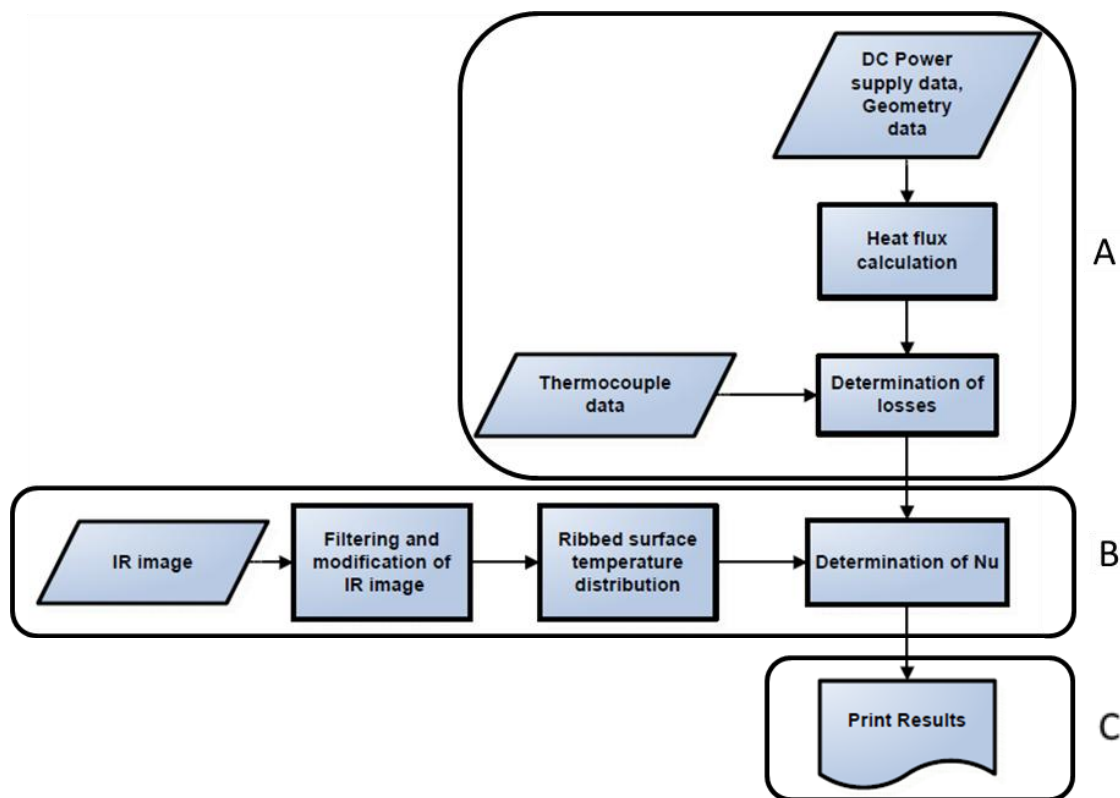


Figure 2.16 Post processing algorithm

2.2.5. Uncertainty Analysis

Regarding the uncertainties of each quantity included in Nusselt number calculations, uncertainty of Nusselt number results can be derived using eqn. 2.11

$$\Delta Nu = \sqrt{\sum_{i=1}^N \left(\frac{\partial Nu}{\partial x_i} \Delta x_i \right)^2} \quad 2.11$$

The derivatives of each quantity is approximated as in eqn. 2.12. In the equation, Δx_i is the uncertainty of the quantity x_i and ΔNu_i is the change in Nusselt number corresponding to variation of each quantity. The assumption is that the change in uncertainty of each quantity is small and that derivative does not change significantly within that small variation.

$$\frac{\partial Nu}{\partial x_i} = \frac{\partial Nu_i}{\Delta x_i} \quad 2.12$$

Hence, the uncertainty equation becomes:

$$\Delta Nu = \sqrt{\sum_{i=1}^N (\Delta Nu_i)^2} \quad 2.13$$

A sensitivity analysis of each quantity is conducted before the uncertainty calculations. The effect of 1% change in each quantity on Nusselt number is calculated and presented in Table 2.1. 1% error on heater voltage and current measurement causes an error of approximately 1% error on Nusselt number. Temperature measurements for loss calculations also effects the Nusselt number calculation around 1%. 1% error on surface temperature measurements cause relatively low error, however the actual errors for the surface temperature measurements are larger than 1%. That will be explained in the following.

Table 2.1 Sensitivities of Nusselt number for Re=20000 case

Quantity	Unit	Value	Sensitivity
Heater voltage	Volt	3.61	1.007%
Heater current	Amper	19	1.007%
Temperature difference of air and heater surface	K	18	0.007%
Temperature difference through plexiglass	K	2.5	1.000%
Thermal conductivity of plexiglass	W/mK	0.19	1.000%
Thermal conductivity of air	W/mK	0.0242	0.007%
Viscosity of air	kg/ms	0.00001846	1.007%
Density of air	kg/m ³	1.177	1.007%

Table 2.2 shows the uncertainties for the Re=20000 case. The most effective parameter on Nusselt number results is the measurement of temperature difference between the heated surface and the air temperature. Overall uncertainty for Nusselt number is found as 2.624%.

Table 2.2 Uncertainties of Nusselt number for Re=20000 case

Quantity	Uncertainty	ΔNu
Heater voltage	0.0742	0.101%
Heater current	0.2225	0.302%
Temperature difference of air and heater surface	1.9185	2.605%
Temperature difference through plexiglass	0.0286	0.039%
Thermal conductivity of plexiglass	-	-
Thermal conductivity of air	-	-
Viscosity of air	-	-
Density of air	-	-
Total		2.624%

The sensitivity and uncertainty for the Reynolds number determination are also calculated. 1% percent pressure measurement sensitivity is found as 0.499% and the uncertainty with actual sensor accuracy is found as 0.125%.

CHAPTER 3

NUMERICAL SETUP

Rib turbulators are implemented to the gas turbine blade cooling channels to increase the convective heat transfer. The ribs create flow separation, reimpingement and secondary flows through the channels, hence it is very important to predict the flow and heat transfer numerically. In addition to literature review, one can quickly glance the works related with the flow and heat transfer inside ribbed ducts [12], [47]–[52].

3.1. Model Geometry and Boundary Conditions

A simplified version of experimental model is built in order to reduce computational cost. As the heat transfer and flow become periodical after 4th rib inside a straight ribbed channel, less number of ribs are implemented to the numerical model [10]. The numerical model is a square channel with 5 and 6 ribs on one wall in the first and second pass, respectively. Numerical model has the same cross section (80×80 mm) and other geometrical parameters like rib height ($e=8$ mm), rib pitch ($P=80$ mm) and U-bend as the experimental setup. The experimental results also validate that phenomena. As in the experimental setup, The description of the numerical geometry is depicted in Figure 3.1.

Inlet velocity measurement of the experimental campaign and constant temperature of 300 K is taken as inlet boundary conditions. At the outlet, pressure outlet is given. Figure 3.2 shows the spanwise averaged, symmetry line and 2D contour of measured inlet velocity profile (m/s) for $Re=20000$ case. Since there is no turbulence intensity measurement, it is given as 5% with an hydraulic diameter of 80 mm [53]. The inter rib surfaces and U turn region of bottom wall is heated with constant heat flux of 400 W/m^2 . Wall boundary conditions are given to the rest of the surfaces.

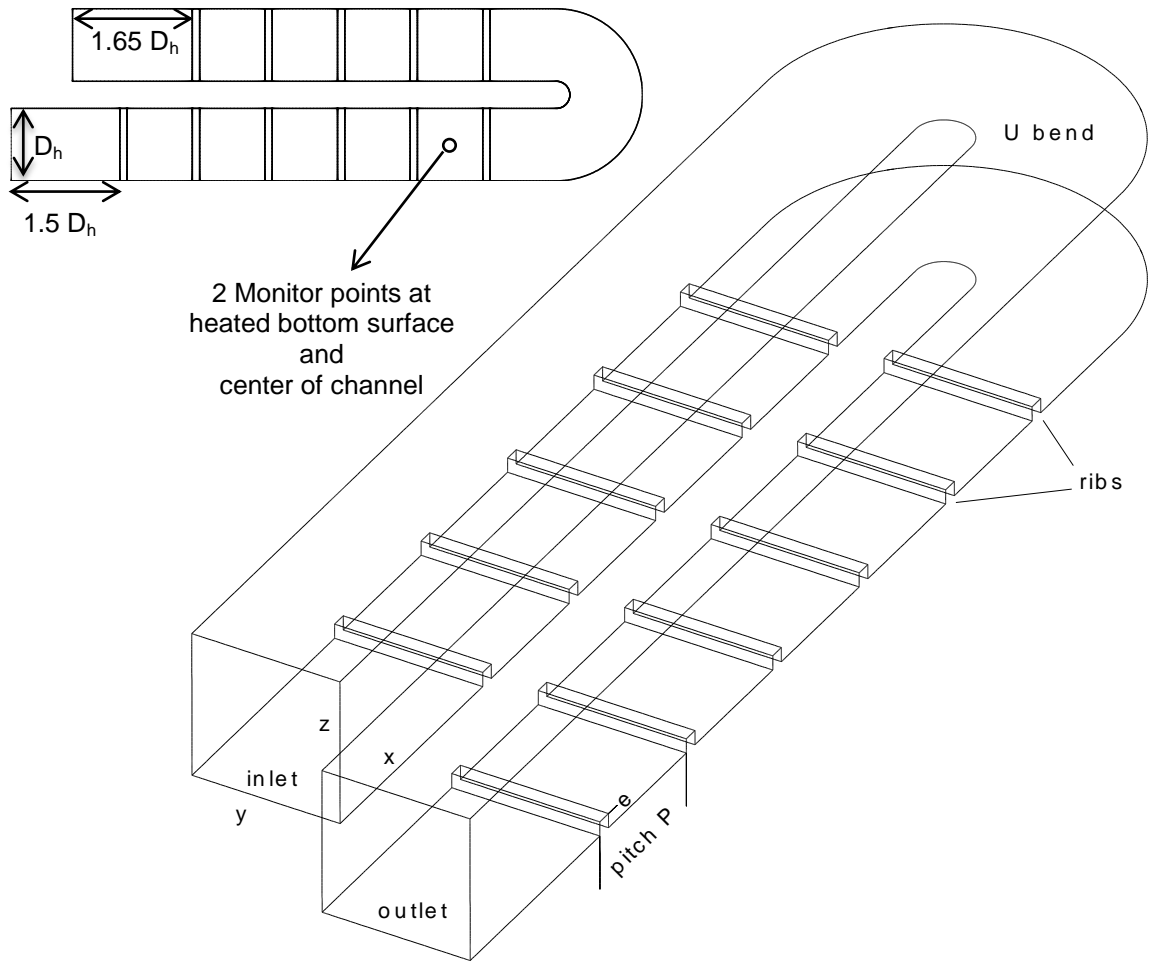


Figure 3.1 Top view and 3D view of numerical setup

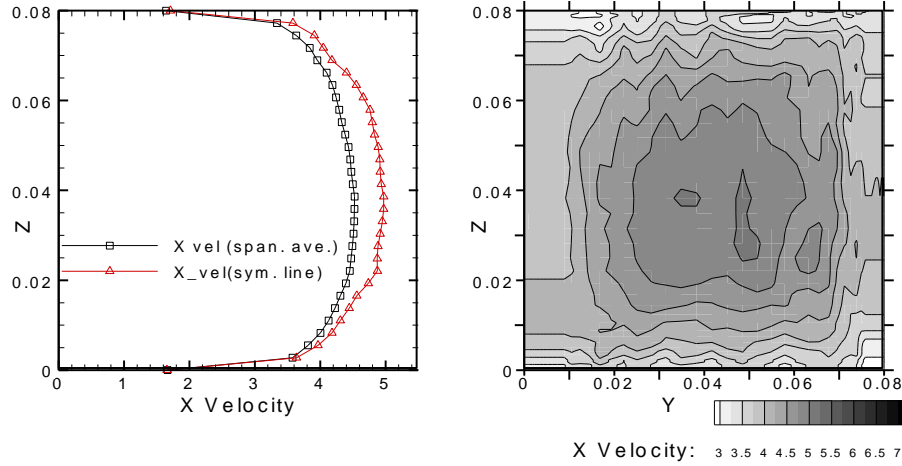


Figure 3.2 Spanwise averaged (left) and 2D contour of streamwise velocity (right)

3.2. Turbulence Modeling

Since the internal geometry of the turbine blades results in a complexity of cooling channel flow (see Figure 1.3). That makes it hard to conduct direct numerical simulations (DNS) for prediction of aero-thermal behaviour inside the channels. Therefore, RANS simulations are generally conducted as they are computationally practical. The realizable $k - \varepsilon$ model, the low Re $k - \varepsilon$ (Yang-Shih), the $v^2 - f$ model, the $k - \omega - SST$ model, Reynolds Stress Model (RSM) are experienced at the numerical campaign. The theories of these turbulence models are described in the following paragraphs. ,

Reynolds Averaging & Boussinesq Approach

Reynolds-averaged Navier–Stokes (RANS) based turbulence models are focused on the mean (ensemble-averaged or time-averaged) and fluctuating components. These components are formed by the methodology based on decomposition of exact Navier–Stokes equations [54]. Decomposed variables can be expressed as:

$$\phi = \bar{\phi} + \phi' \quad 3.1$$

In instantaneous continuity and momentum equations, flow variables in this form are substituted and taken time average to obtain the Reynolds or ensemble averaged momentum eqn 3.2. These equations can be written as (in Cartesian tensor form):

Continuity:

$$\frac{\partial \rho}{\partial t} + \frac{\partial}{\partial x_i} (\rho \overline{u_i}) = 0 \quad 3.2$$

Momentum Equation:

$$\begin{aligned} \frac{\partial}{\partial t} (\rho \overline{u_i}) + \frac{\partial}{\partial x_j} (\rho \overline{u_i u_j}) = & - \frac{\partial \overline{p}}{\partial x_i} + \frac{\partial}{\partial x_j} \left[\mu \left(\frac{\partial \overline{u_i}}{\partial x_j} + \frac{\partial \overline{u_j}}{\partial x_i} - \frac{2}{3} \delta_{ij} \frac{\partial \overline{u_k}}{\partial x_k} \right) \right] \\ & + \frac{\partial}{\partial x_j} (-\rho \overline{u'_i u'_j}) \end{aligned} \quad 3.3$$

These equations have the same general form with the exact Navier-Stokes equations. Besides the ensemble-averaged velocities and other variables, additional terms that represent the turbulent effects, appear. These “ $-\rho \overline{u'_i u'_j}$ ” terms are called as “Reynolds Stresses” [54].

Reynolds stress terms, which are derived after the averaging procedure, are unknown parameters. In order to close these equations, unknown Reynolds stresses must be modeled. Therefore, many different turbulence models were developed which are still in use widely.

Boussinesq approach is still the basis of various developed turbulence models. This approach considers that there is a relation between Reynolds stresses and the mean velocity gradients. In Newton’s viscosity law, the shear stresses are taken to be proportional to the deformation rate. For an incompressible fluid [55]:

$$\tau_{ij} = \mu_{ij} = \mu \left(\frac{\partial u_i}{\partial x_j} + \frac{\partial u_j}{\partial x_i} \right) \quad 3.4$$

In 1887, Boussinesq proposed a hypothesis that the Reynolds stresses might be taken proportional to the mean deformation rate.

$$-\rho \overline{u'_i u'_j} = \mu_t \left(\frac{\partial \overline{u_i}}{\partial x_j} + \frac{\partial \overline{u_j}}{\partial x_i} \right) - \frac{2}{3} \left(\rho k + \mu_t \frac{\partial \overline{u_k}}{\partial x_k} \right) \delta_{ij} \quad 3.5$$

$$k = \frac{1}{2} \left(\overline{u'^2} + \overline{v'^2} + \overline{w'^2} \right) \quad 3.6$$

where, k is the turbulent kinetic energy per unit mass, μ_t is turbulent or eddy viscosity which is not a physical fluid property. It depends on the turbulence level. This means μ_t changes within the fluid flow and depends on the flow conditions. The term δ_{ij} , the Kronecker delta, ensures that the formula gives correct results for normal Reynolds stress terms as well eqn. 3.3, 3.4.

For a concluding remark, it must be mentioned that eventhough this approach has relatively low computational cost so as to compute eddy viscosity, the main drawback of Boussinesq hypothesis is to assume an isotropic turbulence, which is not true exactly and works well for flows dominated by only one of the turbulent shear stresses (such as wall boundary layers, mixing layers, jets etc.) [54].

3.2.1. Realizable k - ε model

Realizable $k - \varepsilon$ model proposed by Shih et al. is a variant model of well known two equation turbulence model “standard $k - \varepsilon$ ” proposed by Launder and Spalding [56] and solves transport equation for the turbulence kinetic energy (k) and turbulence dissipation rate (ε). It is a semi-empirical model and phenomenological considerations and empiricism methods exist in derivation of the model. The realizable model offers alternative approaches about two topics differently from original model:

- The calculation method of eddy viscosity,
- The dissipation rate transport equation that was derived from an exact equation for the transport of the mean-square vorticity fluctuation [54].

The “realizable” term refers the mathematical considerations on Reynolds stresses and turbulence physics that lie behind the model. By combining the Boussinesq relationship (eqn. 3.5) and eddy viscosity formula ($\mu_t = \rho C_\mu k^2 / \varepsilon$) for the normal Reynolds stress terms for an incompressible strained mean flow, following expression can be obtained:

$$\overline{u^2} = \frac{2}{3}k - 2\nu_t \frac{\partial U}{\partial x} \quad 3.7$$

where $\nu_t = \mu_t / \rho$, and the normal stress $\overline{u^2}$ is a positive quantity, it might becomes negative or “non-realizable” when the strain is large enough to satisfy;

$$\frac{k}{\varepsilon} \frac{\partial U}{\partial x} > \frac{1}{3C_\mu} \approx 3.7 \quad 3.8$$

In a similar manner, it can also be shown that the Schwarz inequality for shear stresses ($\overline{u_\alpha u_\beta^2} \leq \overline{u_\alpha^2 u_\beta^2}$; no summation over α and β) might be violated when strain is large. In order to ensure the realizability (this means that to ensure positivity of normal stresses and Schwarz inequality for shear stresses), the appropriate way is to make C_μ coefficient variable and sensitizing it. For instance, C_μ is determined around 0.09 in the logarithmic layer of equilibrium boundary layers and 0.05 in a strong homogeneous shear flows.

The eddy viscosity term is expressed as:

$$\mu_t = \rho C_\mu \frac{k^2}{\varepsilon} \quad 3.9$$

And the variable C_μ coefficient is calculated by following equation:

$$C_\mu = \frac{1}{A_0 + A_s \frac{kU^*}{\varepsilon}} \quad 3.10$$

where A_0 and A_s are model constants and $U^* = \sqrt{S_{ij}S_{ij} + \Omega_{ij}\Omega_{ij}}$.

where Ω_{ij} is the mean rate-of-rotation tensor viewed in a moving reference frame with the angular velocity ω_k .

3.2.2. Low Reynolds Yang-Shih Model

Transport equations of low-Reynolds number k - ε turbulence models:

$$\frac{Dk}{Dt} = \frac{\partial}{\partial x_j} \left[\left(\nu + \frac{\nu_t}{\sigma_k} \right) \frac{\partial k}{\partial x_j} \right] + P_k - \tilde{\varepsilon} - D \quad 3.11$$

$$\frac{D\tilde{\varepsilon}}{Dt} = \frac{\partial}{\partial x_j} \left[\left(\nu + \frac{\nu_t}{\sigma_\varepsilon} \right) \frac{\partial \tilde{\varepsilon}}{\partial x_j} \right] + C_{z1} f_1 \frac{1}{T_t} P_k - C_{z2} f_2 \frac{\tilde{\varepsilon}}{T_t} + E \quad 3.12$$

where $P_k = -u_i u_j \frac{\partial U_i}{\partial x_j}$ is the production of turbulent kinetic energy and $\nu_t = C_\mu f_\mu k^2 / \varepsilon_1$.

C_μ is constant and f_μ is damping function. T_t is a turbulent time scale, $\tilde{\varepsilon}$ is the modified isotropic dissipation rate, D and E are near wall correction functions for k and ε equations.

The dumping functions that are used in low-Re-YS model:

$$f_\mu = (1 + 1 / \sqrt{\text{Re}_t}) \times \left[1 - \exp \left[\begin{array}{c} -1.5 \times 10^{-4} \text{Re}_y \\ -5.0 \times 10^{-7} \text{Re}_y^3 \\ -1.0 \times 10^{-10} \text{Re}_y^5 \end{array} \right] \right]^{0.5} \quad 3.13$$

$$f_1 = \frac{\sqrt{\text{Re}_t}}{1 + \sqrt{\text{Re}_t}} \quad 3.14$$

$$f_2 = \frac{\sqrt{\text{Re}_t}}{1 + \sqrt{\text{Re}_t}} \quad 3.15$$

Where $\text{Re}_t = \frac{k^2}{\nu \varepsilon}$, $\text{Re}_y = \frac{y k^{1/2}}{\nu}$, $y^* = \frac{y u_\varepsilon}{\nu}$, $u_\varepsilon = \frac{(\nu \varepsilon)^{0.25}}{\nu}$

D and E term along the wall: $D = 0$, $E = \nu \nu_t \left(\frac{\partial^2 U}{\partial y^2} \right)^2$.

Model Constants: $C_\mu = 0.09$, $C_{\varepsilon 1} = 1.44$, $C_{\varepsilon 2} = 1.92$, $\sigma_k = 1.0$, $\sigma_\varepsilon = 1.3$.

3.2.3. v2f Model

For some cases, the eddy viscosity models are not satisfactory since, they might overpredict the turbulent kinetic energy and are not sensitive to the interaction between streamline curvature and anisotropy. In addition to this, the Reynolds Stress Model is more detailed model the turbulent effects that other RANS models can not model, but it is more complex, computationally expensive and sometimes numerically unstable. At that point, the $v^2 - f$ turbulence model is a good alternative that is similar to standard $k - \varepsilon$ model and it accounts near wall anisotropy and non-local pressure strain effects additionally.

The $v^2 - f$ is a four-equation turbulence model and solves transport equations for turbulence kinetic energy (k), turbulence dissipation rate (ε), velocity variance scale ($\overline{v^2}$) and the elliptic relaxation function (f). Here, velocity variance scale can be considered as the velocity fluctuation normal to the streamlines and it provides right scaling in representing the damping of turbulent transport close to the wall. It is a feature that turbulence kinetic energy can not provide.

The eddy viscosity term in $v^2 - f$:

This model uses velocity variance scale (and turbulent time scale evaluated in the model steps) instead of turbulent kinetic energy to evaluate eddy viscosity term. The expression for the eddy viscosity is given as $\mu_t = \rho C_\mu \overline{v^2} T$.

3.2.4. k- ω -SST Model

Shear Stress Transport k- ω model (developed by Menter), uses the standard k- ω formulation at near wall regions and the k- ε formulation in the far fields and blending these model efficiently. In order to achieve that, k- ε to k- ω conversion operation is done.

- Conversion operation from $k - \varepsilon$ to $k - \omega$ model is done by multiplying a blending function. When the blending function is “1” at near wall regions it activates standard $k - \omega$ model and “0” away from the walls, it activates $k - \varepsilon$ model.
- The specific turbulence dissipation rate term (ω) includes damped cross-diffusion derivative term in SST model.
- For taking account of transport of the turbulent shear stress, turbulent viscosity definition is modified.
- The model constants are different for both $k - \omega$ models.

The eddy viscosity is expressed as;

$$\mu_T = \frac{\rho k}{\omega} \frac{1}{\max \left[\frac{1}{\alpha^*}, \frac{SF_2}{a_1 \omega} \right]} \quad 3.16$$

where S is the strain rate magnitude and

$$\sigma_k = \frac{1}{F_1/\sigma_{k,1} + (1 - F_1)/\sigma_{k,2}} \quad 3.17$$

$$\sigma_\omega = \frac{1}{F_1/\sigma_{\omega,1} + (1 - F_1)/\sigma_{\omega,2}} \quad 3.18$$

$$\alpha^* = \alpha_\infty^* \left(\frac{\alpha_0^* + \text{Re}_t/R_k}{1 + \text{Re}_t/R_k} \right) \quad 3.19$$

where $\text{Re}_t = \frac{\rho k}{\mu \omega}$, $R_k = 6$, $\alpha_0^* = \frac{\beta_i}{3}$, $\beta_i = 0.072$.

The blending functions F_1 and F_2 that are used for combining the models, are given as;

$$F_1 = \tanh(\Phi_1^4) \quad 3.20$$

$$\Phi_1 = \min \left[\max \left(\frac{\sqrt{k}}{0.09 \omega y}, \frac{500 \mu}{\rho y^2 \omega} \right), \frac{4 \rho k}{\sigma_{\omega,2} D_{\omega}^+ y^2} \right] \quad 3.21$$

$$D_{\omega}^+ = \max \left[2 \rho \frac{1}{\sigma_{\omega,2}} \frac{1}{\omega} \frac{\partial k}{\partial x_j} \frac{\partial \omega}{\partial x_j}, 10^{-10} \right] \quad 3.22$$

$$F_2 = \tanh \left(\Phi_2 \right) \quad 3.23$$

$$\Phi_2 = \max \left(\frac{\sqrt{k}}{0.09 \omega y}, \frac{500 \mu}{\rho y^2 \omega} \right) \quad 3.24$$

where y is the distance to the next surface and D_{ω}^+ is the positive portion of the cross-diffusion term.

Cross-Diffusion Term:

As mentioned in pervious paragraphs, SST model blends two turbulence models $k - \varepsilon$ and $k - \omega$. In order to blend these models, a cross diffusion term is created.

$$D_{\omega} = 2 (1 - F_1) \rho \frac{1}{\omega \sigma_{\omega,2}} \frac{\partial k}{\partial x_j} \frac{\partial \omega}{\partial x_j} \quad 3.25$$

3.2.5. Reynolds Stress Models

The Reynolds stress model is detailed RANS turbulence model. Instead of the isotropic eddy-viscosity approach, the RSM solves transport equations for individual Reynolds stresses and the turbulent dissipation rate equation to close Reynolds-averaged Navier-Stokes equations. That means that one must solve seven transport equations in 3D simulations. For complex flows, RSM has potential to get more accurate result than one or two equation models. However, RSM predictions is still limited by the assumptions to model terms in transport equations for the Reynolds stresses. If the computational expense and obtained results in the RSM simulations are examined, the RSM might not give better results than simpler models in all flow conditions. But,

anisotropy in the Reynolds stresses is of interest, the RSM has an important role while modeling the turbulence.

The eddy viscosity term is evaluated in the same manner as in the $k - \varepsilon$ model:

$$\mu_t = \rho C_\mu \frac{k^2}{\varepsilon} \quad 3.26$$

where C_μ has a constant value of 0.09.

3.3. Numerical Approach and Mesh Generation

In this part, the approach for grid generation and turbulence models for the case is explained. The details of selection of turbulence model is illustrated regarding the literature.

Numerical analysis are conducted with ANSYS FLUENT 14.0 software. Steady state solutions were obtained with pressure based solver algorithm. SIMPLE (Semi implicit method for pressure linked equations) algorithm is selected for pressure velocity coupling. PRESTO (Pressure staggering option) is selected for spatial discretization. Second order discretization is used for all equations. Enhanced wall treatment is activated for the Realizable k- ε Model and the Reynolds Stress Model.

For all numerical analysis, computational domain consists of fully structured multiblock mesh structure with refinement near the walls and rib vicinities. In order to capture the boundary layer flow, y^+ is set below unity for all surfaces with an exception of the surface of the first rib at the second pass, which has y^+ value of approximately 1.7. Contours of y^+ values for ribbed case are shown in Figure 3.3.

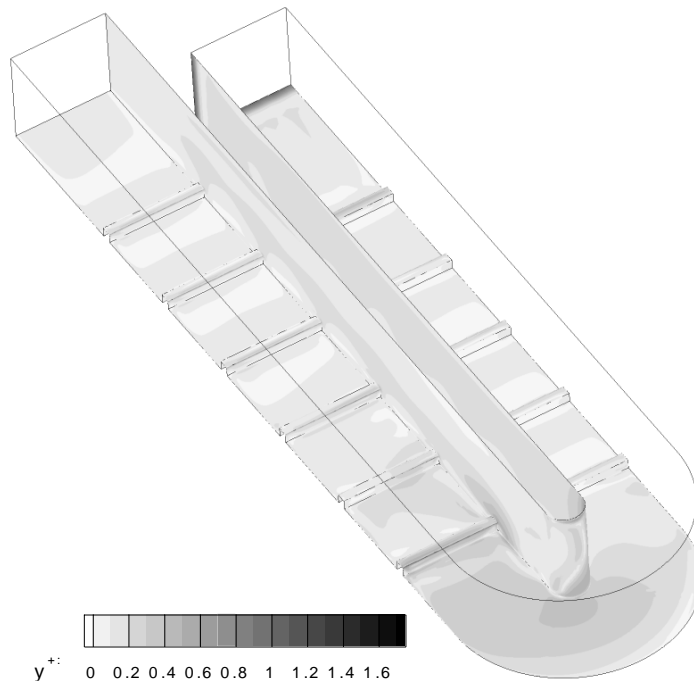


Figure 3.3 y^+ contours of ribbed channel model

Mesh independency is performed for $k-\epsilon$ and YS turbulence models for ribbed channel model. The grids of smooth cases are generated with a similar logic that of the ribbed models. Inter rib area averaged Nu results of two models are presented in Figure 3.4.

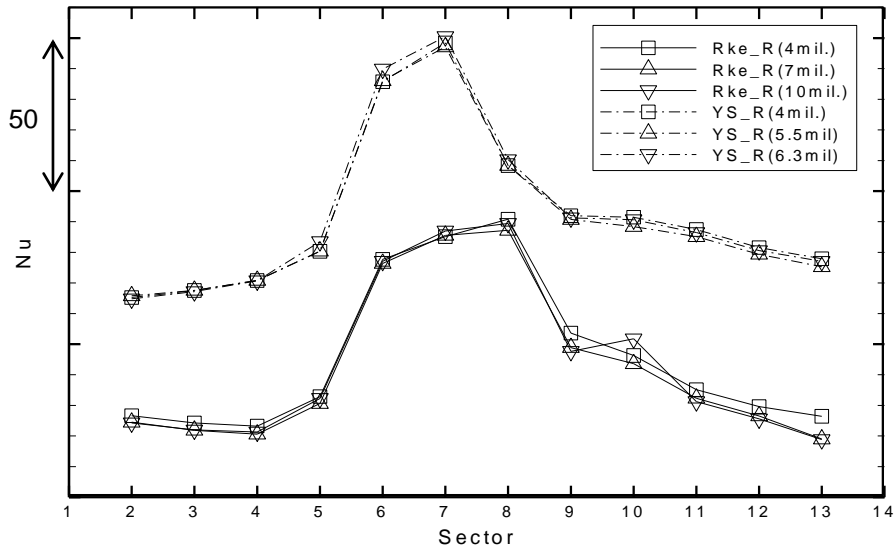


Figure 3.4 Mesh independency for Rke and YS models

First cell thickness is set as 0.25 % of the rib height and grid is generated with a growth rate of 1.2. Figure 3.5 shows the mesh structure for inter rib and turn regions. Figure 3.6 shows the selected mesh structures for the analysis.

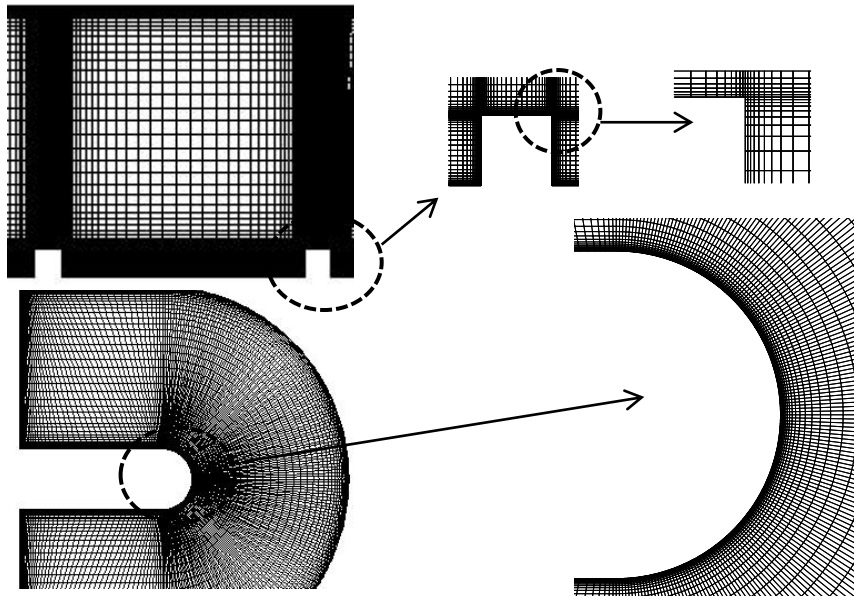


Figure 3.5 Mesh structure at inter rib and turn regions

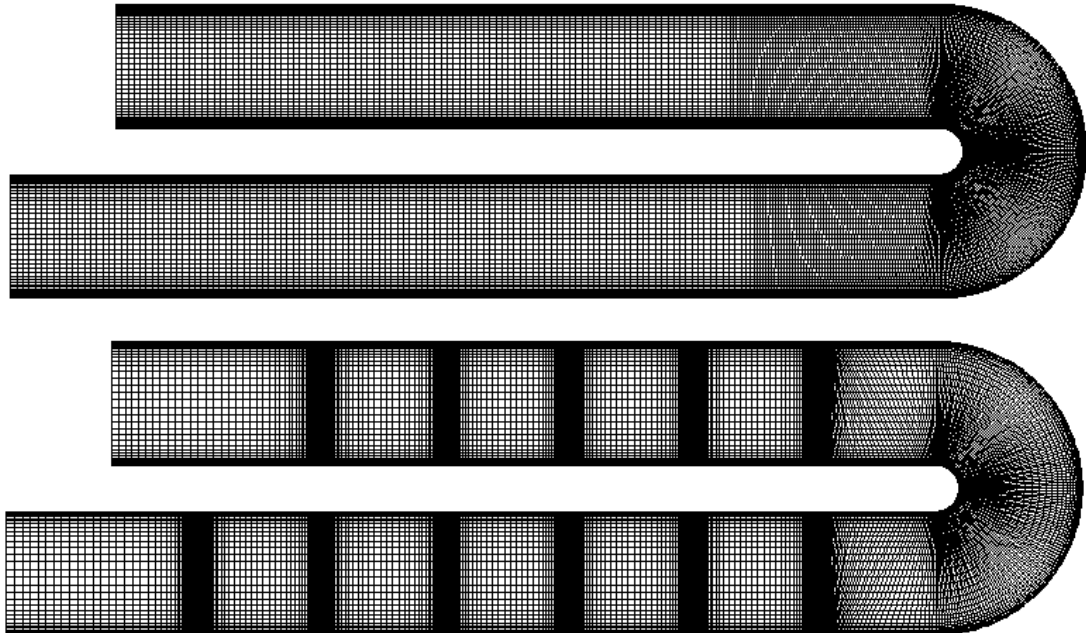


Figure 3.6 Mesh structure for smooth(top) and ribbed(bottom) cases

Table 3.1 shows the vertical, horizontal and streamwise node numbers for the selected and finest mesh structures. There are 4.2 and 2.5 millions of elements for ribbed and smooth case, respectively. Node numbers in 3 direction are presented in Table 3.1.

Table 3.1 Number of nodes for mesh generation (ribbed case)

Block node number	# of nodes (applied mesh)	# of nodes (fine mesh)
Vertical	73	110
Horizontal	54	70
Streamwise	1157	1530
Total	4.2 million	10.1 million

The convergence criteria was 10^{-3} for continuity, 10^{-4} for velocity, k and ϵ , and 10^{-6} for energy results. Two different monitor points are located in the second pass in order to trace the convergence of the simulations. Static temperature at the heated surface and streamwise velocity at the channel center are monitored. The monitor points are located at the points The convergence criteria for all cases is 1×10^{-6} for the control points. The final solutions are judged when the values at the monitor point doesnot change more 10^{-4} %. The convergence and location of control points are shown in Figure 3.7.

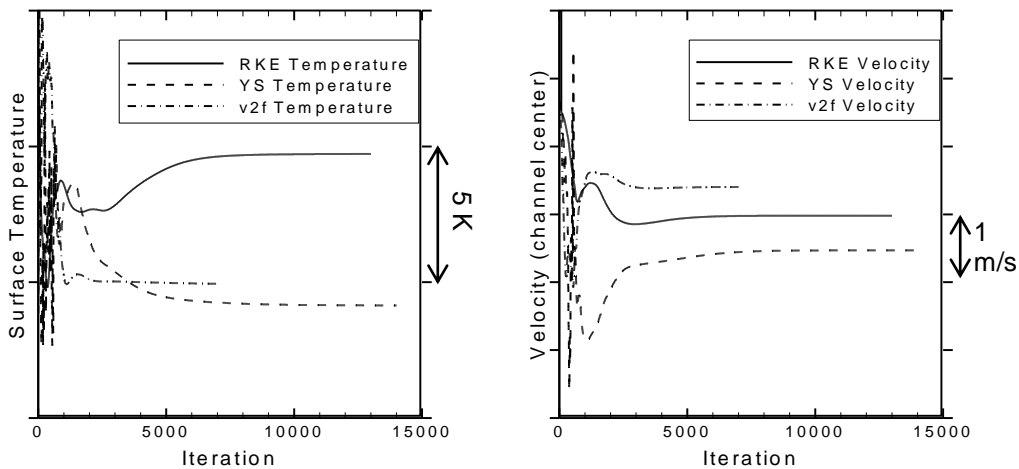


Figure 3.7 Convergence at monitor points

CHAPTER 4

HEAT TRANSFER RESULTS AND DISCUSSION

Measured Nusselt number distribution of two pass ribbed and smooth channel configurations and comparison with numerical analysis are presented. The heat transfer behaviour of U-bend section and the second pass are addressed. The heat transfer characteristics at Inter rib area, variation of averaged Nusselt number and the heat transfer enhancement factor (Nu/Nu_{sm}) along the channel are the prime focus of the investigation. Numerical simulations are also performed in order to have a better understanding of the flow field at the interested regions. The results for the heat transfer predictions with five turbulence models are addressed.

4.1. Heat Transfer in Smooth and Ribbed Channels

In order to assess the heat transfer enhancement of ribbed roughened cooling channel, Nusselt number distribution of a smooth (unribbed) channels are obtained experimentally as a reference. The tests are conducted at three Reynolds numbers of 20000, 35000, and 50000 calculated based on channel dhdyrolic diameter and the mean inlet velocity. As described previously in data reduction section (2.3), the results of area averaged Nusselt number measurements are depicted in Figure 4.1 for smooth and rib roughened configurations at Re 20000. Although there is no rib presented in the smooth

channel, the average nusselt number is calculated respecting the regions presented for the rib roughened case.

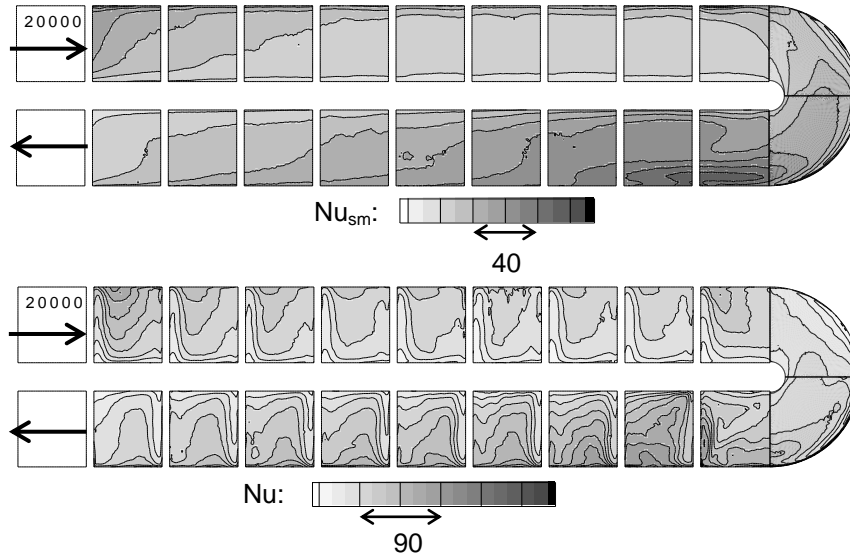


Figure 4.1 Smooth and ribbed channel Nusselt Number distribution ($Re = 20000$)

In the first rib section redeveloping of flow results in a high Nu values up to 5th - 6th inter rib space. Then, flow becomes periodical and present almost constant heat transfer coefficient up to the U bend section. The results also show that near the outer wall region, the Nu appears to be higher compared to the near inner wall region. This can be explained by two dimensional heat transfer of inner wall region. The heater is intalled as a single piece which results in a heat flux generation below the mid-wall. The wall is made of plexiglass hence the conduction through the midwall is not well established. Therefore, some part of the generated heat flux goes in spanwise direction so more heat flux directed to the near inner wall region.

However the problem disappears when the heat transfer enhancement is calculated. For both (smooth and rib roughened) cases, Nusselt number shows as an increasing character along the turn region. The reason of variation of Nu in U-turn can be mainly explained

by the formation of Dean vortex pairs [53, 54]. Calculated Dean numbers for the Reynolds numbers of 20000, 35000, and 50000 are 24121, 42212, and 60302, respectively (eqn. 4.1).

$$De = Re \left(\frac{D_h}{R} \right)^{1/2} \quad 4.1$$

Area averaged Nusselt number distributions are plotted for three Reynolds numbers in Figure 4.2. When the mean flow velocity increases, the overall Nu trend doesnot change characteristics but Nu of each section raises proportionally. Nu starts to increase when the flow enters the u-turn and makes a peak at the 14th rib area. The peak value of heat transfer coefficient can be explained by a combined effect of ribs and turn induced flow. Stream traces over the turn region and downstream are presented in the numerical simulation results part. The effect of u-turn section continues through the whole second pass.

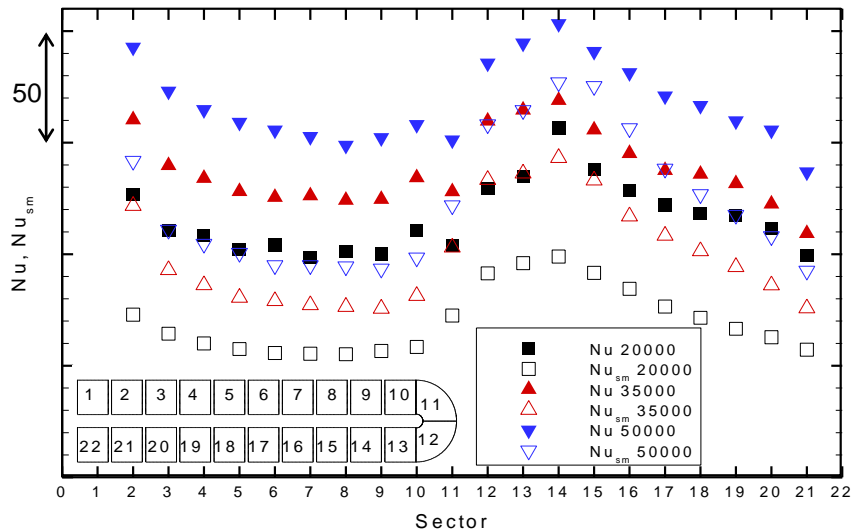


Figure 4.2 Area Averaged Nu and Nu_{sm} results

Normalized Nusselt number distributions are presented in Figure 4.3 and Figure 4.4 The heat transfer enhancement due to the reattachment of flow after ribs are observed at each

inter rib space for all cases. The length required for flow re-development varies with Reynolds number. At $Re=20000$ and 35000 , flow becomes periodic after 4 inter rib space whereas at $Re=50000$ flow re-development last 5 inter rib space. The heat transfer coefficient reaches its high values always at the flow re-development regions of 1st and 2nd flow channels. Since the smooth configuration heat transfer increases because of the turn induced Dean vortex structures and the difference between the ribbed and smooth channel configurations gets weaker.

The heat transfer enhancement factor is good indicator to evaluate the heat transfer performance of the rib roughenned channels. Therefore, the enhancement factor is calculated by dividing the Nu results of ribbed roughenned configuration to the smooth configuration. The 2D contour plot of enhancement factor distribution is presented in Figure 4.4. $Re=20000$ case gives the highest heat transfer enhancement among three cases. No significant diffence is observed between $Re=35000$ and $Re=50000$ cases. Although, the flow re-development regions result in high Nu values, the enhancement factors at those regions are relatively lower compared to the periodic flow regions. Similar conclusion is also true for the U turn section. In contrast to the high Nu value of U turn region, the heat transfer enhancement reaches its minimum value. That implies the fact that turning effects can contribute the heat transfer immediately for smooth channel and Nu values drops. Downstream of the u-turn section, the enhancement factor starts increasing again paralel to the flow establishment. At $Re=20000$, flow re-development is complited at the end of the 2nd channel since the enhancement values of last two inter-rib space are close and similar to the one of the 1st channel periodic flow region. However, at higher Re values, the flow needs more space to become fully developed in the 2nd channel.

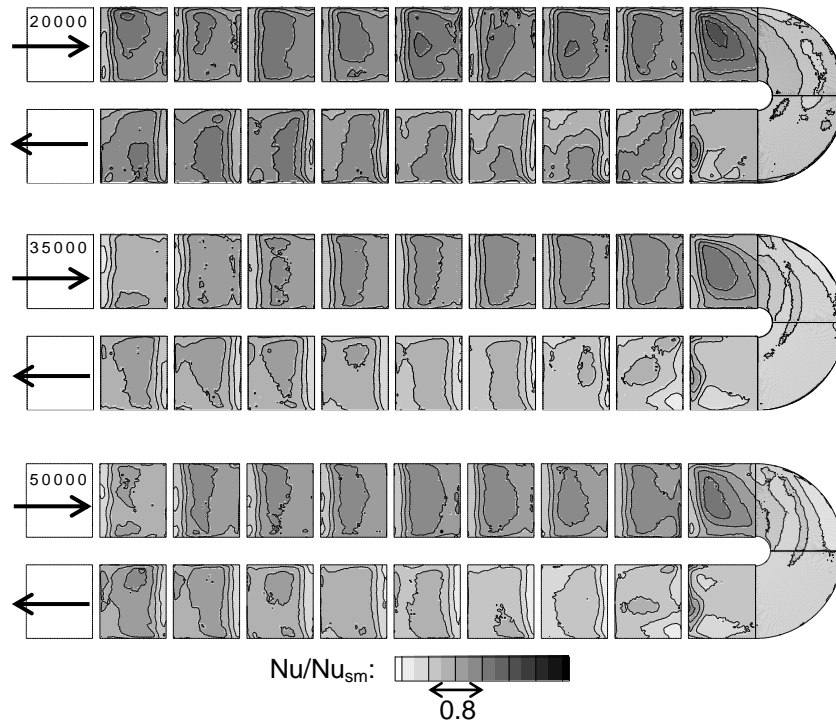


Figure 4.3 Ribbed channel Nu/Nu_{sm} distribution ($Re = 20000, 35000, \& 50000$)

Inter rib area averaged Nu/Nu_{sm} distribution through the cooling channel model is plotted in Figure 4.4 for all cases. $Re=20000$ case gives the the highest heat transfer enhancement among three cases. There is no significant diffence between $Re=35000$ and $Re=50000$ cases. In the 1st passage, Nu/Nu_{sm} values increases constantly through the chanel and no periodical heat transfer enhancement is obtained. At the turn section, the heat transfer enhancement drops rapidly about 20-30% starting with 11th sector. That implies the fact that turning effects can contribute the heat transfer immediately. The effect of ribs at the 1st pass still reaches the turning part. Smooth configuration heat transfer is also increasing because of the turn induced Dean vortex structures and the difference between the ribbed and smooth channel configurations gets weak. cannot reach at the turn section and the smooth Starting with the turn effect, Nu/Nu_{sm} values are decreasing drastically. That sharp decrease shows that unribbed turn area shows the

same heat transfer behaviour for smooth and ribbed cases. In other words, the ribs at the upstream channel have a little effect on U turn section when compared to straight parts. Another conclusion is that the heat transfer performance of ribbed duct relative to smooth one drops with Reynolds number increase.

In the 2nd passage, the Nu/Nu_{sm} increases constantly due to the decreasing effect of heat turning geometry. Rib induced heat transfer becomes dominant at about 18th and 19th sector. The heat transfer enhancement level of 1st passage is almost obtained at that sectors for $Re=20000$ case. For higher Reynolds number cases, the heat transfer enhancement continues redeveloping through the secon pass and cannot reach the value of the 1st passage fully developed and periodical levels. This concludes that the flow with lower velocity redevelops and reaches the 1st straight part level quicker than the cases with high velocity.

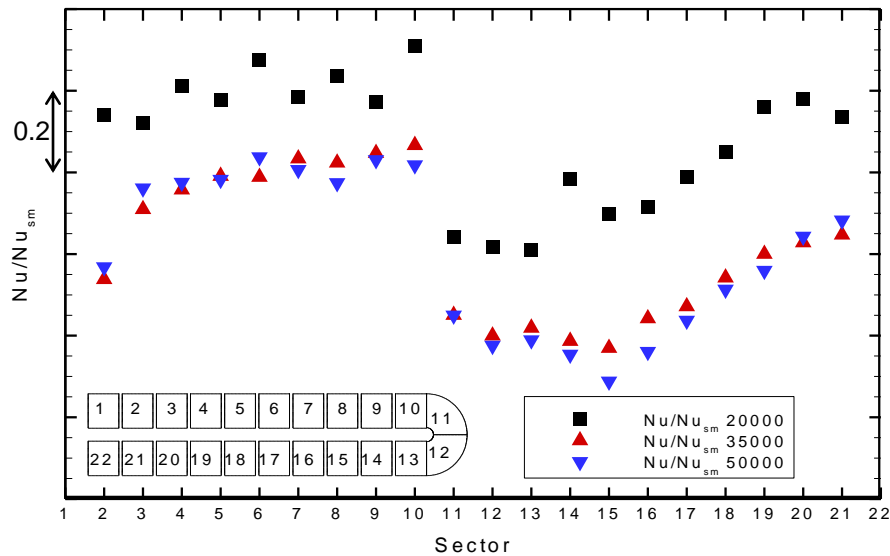


Figure 4.4 Area averaged Nu/Nu_{sm} Results ($Re = 20000, 35000, \& 50000$)

4.2. Comparison with Numerical Predictions

Performance of 5 turbulence models are compared with the experimental Nusselt number results of the ribbed case for a single inter rib space. Low Re YS, v2f and realizable k- ϵ models are selected later on for smooth channel simulations. The numerical results of ribbed channel are normalized by using the results of smooth channel. Numerical analysis are conducted to find best numerical setup and analyze the relation between the heat transfer and flow field of the 2 pass channel at Re=20000. The flow field downstream of a single rib solved by YS and v2f models is compared with the literature. Finally, Nu, Nu_{sm} and heat transfer enhancement factor (Nu/Nu_{sm}) results are analyzed.

In Figure 4.5, spanwise averaged Nusselt numbers in flow direction over 4th inter rib space are plotted for all turbulence models and experiments. Additionally, the Nu distribution of the channel mid-line (symmetry plane) is plotted for some cases in order to characterise the difference between both approaches. v2f model results in the best approximation to the real values. It predicts well the flow re-development region but under predicts when there is a recirculation. SST model is also provides the same trend then results of v2f model but under-predicts the results. YS model over-predicts the Nu numbers whereas all others under-predicts the heat transfer coefficient. YS model is the only model where there is clear difference between mid-line and averaged results. This difference means that the secondary flows generated at the edges of bottom wall and lateral walls are stronger than the other models. The location of the maximum heat transfer coefficient also corresponds to the flow re-attachment varies depends on the turbulence model. Re-attachment distance from the leading rib wall is about 3e for the experiments and YS model, and 2.5e for RKE model. The re-attachment location is determined at 5e from the downstream of leading rib for v2f model.

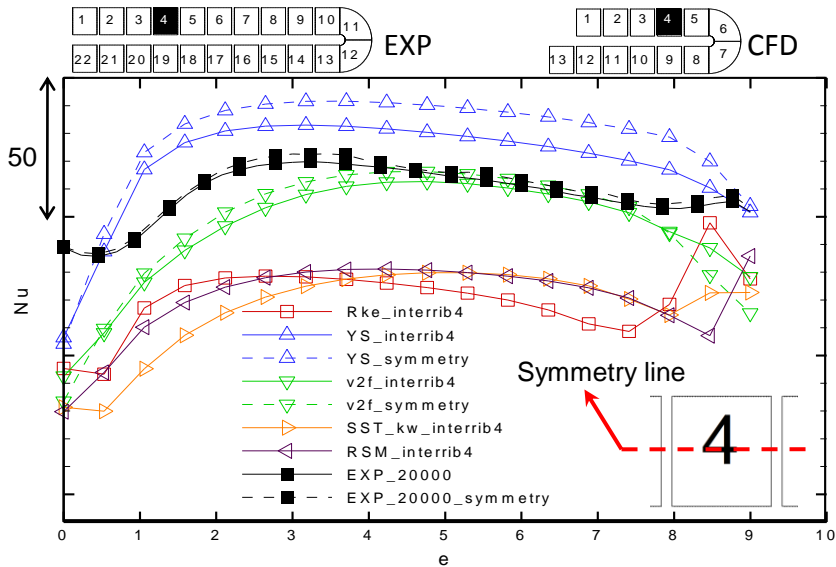


Figure 4.5 Spanwise averaged Nu along 4th inter rib

Streamtraces along 4th inter rib space are presented for v2f and YS models in

Figure 4.6. The size of the circulation region is directly related with the flow re-attachement. Inter rib region velocity measurements of Rau et al. [59] at a height of 0.1e from the heated wall shows that the flow impingement occurs at about 3.5e from the rib rear wall for $P/e=9$ and $Re=30000$. However in the simulation, it is observed that the V2f model predicts much wider recirculation region downstream of the rib whereas the YS model prediction of the recirculation region seems more reasonable.

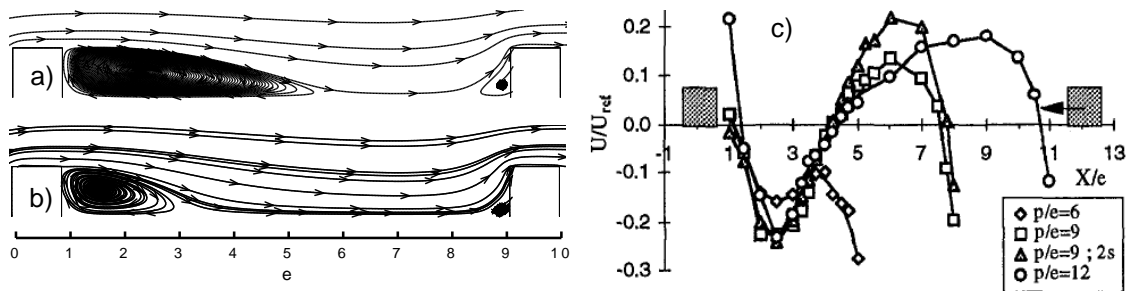


Figure 4.6 4th inter rib streamtraces for v2f (a) and low Re(b) (low) models and [59](c).

The overall area averaged Nusselt number distribution is compared in Figure 4.7. YS and v2f models are in relatively better agreement at the straight parts of the channel when compared to other turbulence models. On the other hand, they overpredict the Nusselt number at turn region. YS and v2f models cannot capture the decreasing heat transfer behaviour through the 1st pass, however, RKE, k- ω SST and RSM models shows a decreasing pattern. Consequently, Rke, k- ω SST and RSM models underpredicts the heat transfer inside a straight channel with 90 deg ribs. In other words, seperated flow heat transfer can be estimated with YS and v2f models whed these five models are considered. The heat transfer increase because of rib implementation and U turn geometry at the downstream of the bend is not captured by any of these models. Only v2f model shows just a small increase and the heat transfer trend along the channel model makes a local maximum at the 9th region as in the experiment results. In addition, all of the results reveals the constant decrease of heat transfer along the second channel and heat transfer not become periodical similar to the experiment.

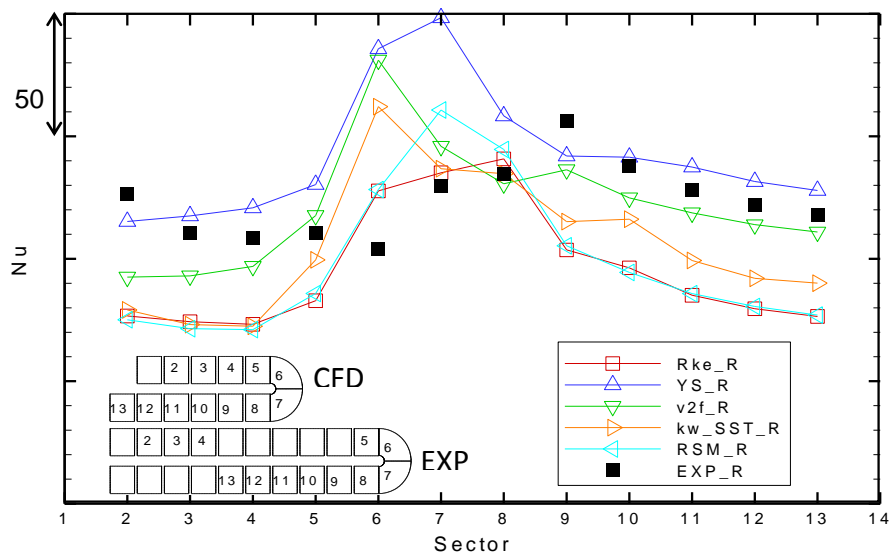


Figure 4.7 Inter rib area averaged Nu results

Three of five turbulence models are selected for smooth wall computations and the results are compared with the one of the experiments. Area averaged Nu results along the smooth channel configuration is illustrated in Figure 4.9. Rke and YS models are in a good agreement with the experimental results at the 1st passage. However, when flow enters the u-turn and in the 2nd channel, all models fails to predict the correct heat transfer coefficients. Rke is the most succesfull to capture the trend but it overpredicts the Nu value. Additionally, the Nu number decays more rapidly compared to the measurements. The $\nu 2f$ model shows totally different physic than the real case in whole channel.

Turbulence intensity is checked for the ribbed case with YS model. YS1 is the selected configuration in which turbulence intensity at the inlet is set as 5% with 80mm hydraulic diameter. In YS2, turbulence intensity is set as 5% with 30mm turbulent length scale. In YS3, is set as 1% with 80mm hydraulic diameter. YS2 is does not cause any significant difference. However, YS3 configuration results in much lower predictions at the 1st pass and turn, small deviations at the 2nd ass. Nu decreases more rapidly at the 2nd pass at the YS3 setting when compared to YS1.

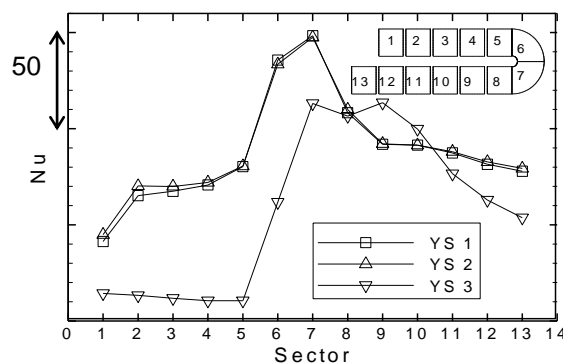


Figure 4.8 Turbulence intensity check for YS model

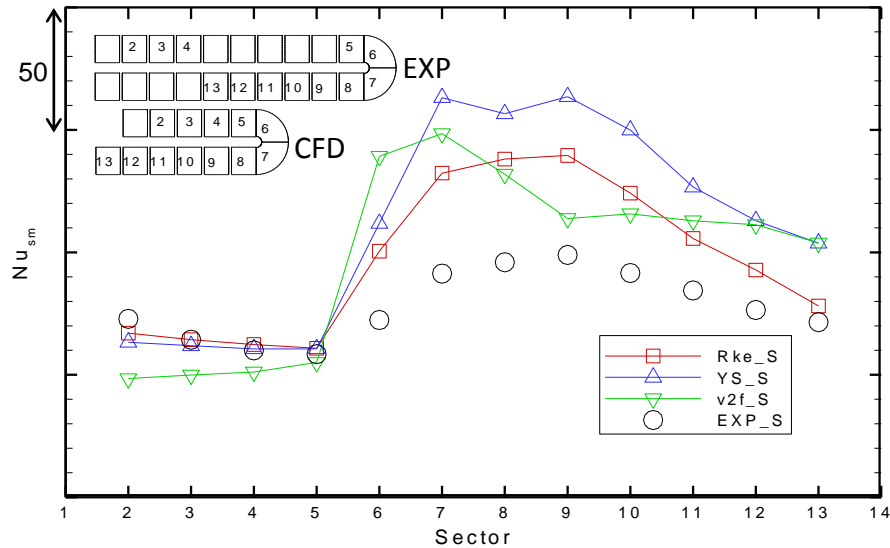


Figure 4.9 Inter rib area averaged Nu_{sm} results

Nu , Nu_{sm} of the Rke, v2f and YS model are demonstrated in Figure 4.10 In smooth wall configurations, heat transfer distribution is almost constant at the 1st passage. Heat transfer increase at the surfaces near the outer wall at the turn region shows up because of the higher momentum fluid impinges at the outer regions [33]. In all smooth channel simulations, sharp heat transfer increase occurs at the outer region of just downstream of the U turn. The flow coming from the turn region impinges at the outer wall and creates the highest heat transfer region for the whole smooth channel. U turn effect on heat transfer diminishes relatively earlier at the v2f model results.

At the 1st passage, all models show almost periodic distribution of heat transfer coefficient after second rib. At the turn region, turning geometry has a significant effect and Dean vortices are generated due to the bend. That local heat transfer increase is because of the impingement of flow to the heated surface and the complex flow structure due to the ribs and turn geometry. Heat transfer coefficient increases near outer wall. All turbulence models have different location for maximum local heat transfer coefficient at u-turn section. For all three turbulence models, there is a local increase in Nusselt

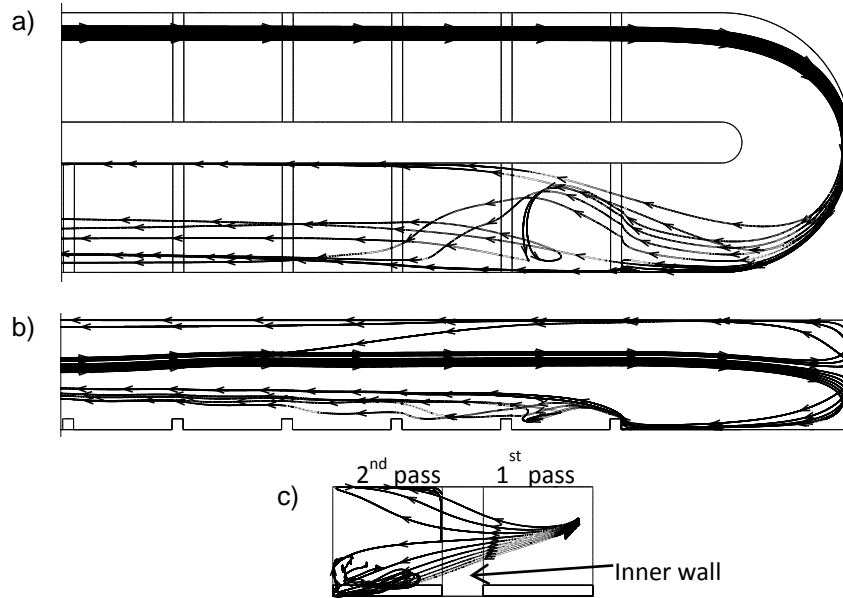


Figure 4.11 Stream traces at the bend region a)top view, b)front view, c)right view

Relatively lower Nusselt number distribution is obtained at the inner wall vicinity at just downstream of the U-bend for both experimental and numerical simulations except the v2f model. That decrease can be attributed to the circulating region near the inner wall, [33].

Unique Nu distribution at 8th and 9th inter rib spaces can be attributed to the different flow behaviour as demonstrated in Figure 4.11. The streamtraces released from 1st pass around 60% height are shown in different views of reference. The flow splits towards the top and heated bottom surfaces while passing the U bend region. At the downstream of the bend, a relatively complex flow structure is observed at 8th and 9th inter rib spaces. Flow goes towards the inner wall and circulates around the 8th inter rib area. After 3rd rib, heat transfer pattern gets relatively similar to the one of 1st passage. However, difference of flow field due to U turn still be effective through the whole 2nd passage by creating an asymmetrical heat transfer distribution. The Nu distribution close to the outer side wall is observed to be higher than the average values for all numerical results.

Normalized heat transfer results of ribbed channel results shows the augmentation of heat transfer due to rib implementation to the cooling duct. Figure 4.12 presents the normalized heat transfer distribution and inter rib area averaged results over the channel model. The outputs are also compared with the experimental data.

The effect of ribs at the 1st pass still reaches the turning part. That sharp decrease at the bend shows that unribbed turn area shows the similar heat transfer behaviour for smooth and ribbed cases. In other words, the ribs at the upstream channel have less significant effect on U turn section when compared to the 1st pass. Nu/Nu_{sm} distribution is relatively lower at the 2nd passage. Nu/Nu_{sm} increases constantly due to the redevelopment of flow to the rib roughened channel. The heat transfer enhancement level of 1st passage is almost obtained at 12th - 13th sectors for the experiments. For higher Reynolds number cases, the heat transfer enhancement increases all along the 2nd pass and cannot reach to the value of the 1st passage developed level.

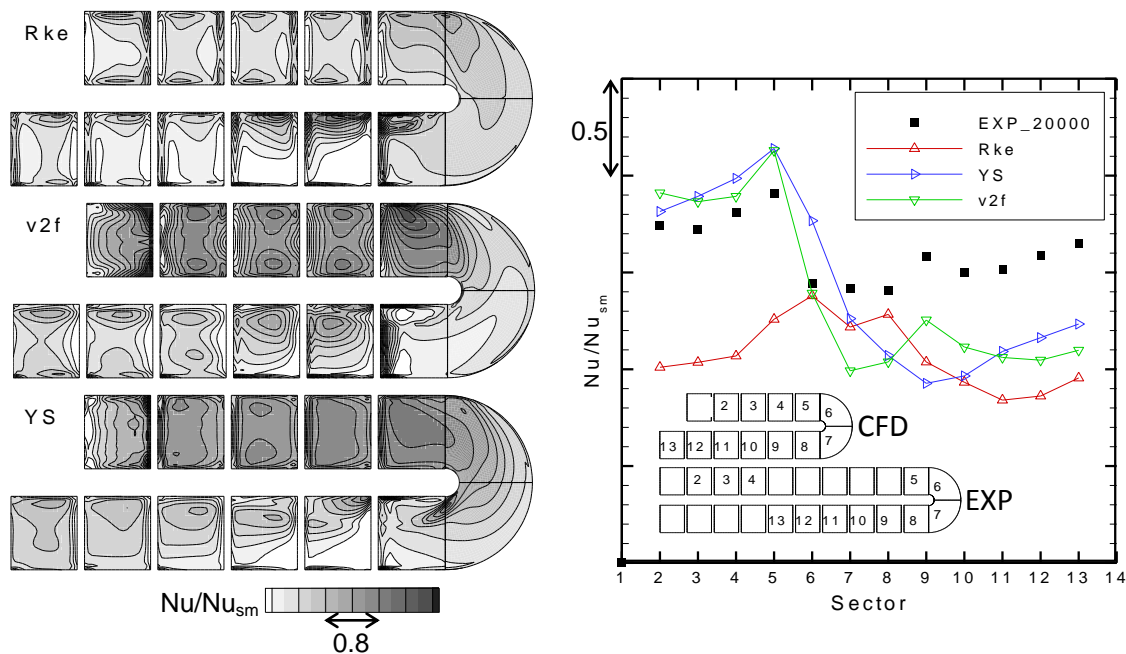


Figure 4.12 Nu/Nu_{sm} distributions and spanwise averaged results ($Re=20000$)

Heat transfer inside the channel is augmented about 1.5-2 times at the 1st passage and heat transfer augmentation slightly increases in the streamwise direction. Although the Nu distribution is well predicted by the Rke and YS model compared to the v2f, the cooling effectiveness results shows a different conclusion. In the 1st channel the cooling effectiveness results of YS and v2f models get close to the experimental results. The Rke model fails to predict the effectiveness value correctly because it estimates high level of Nu for the smooth channel case. On the other hand, Rke model is quite successful when the cooling effectiveness is predicted at the u-turn region. In the 2nd pass, all three models underpredicts the experimental results. The overall trend of the cooling effectiveness of the 2nd channel is only captured by YS turbulence model. The local maximum at the second inter rib region at the 2nd pass (9th inter rib area) can be captured by only v2f model.

In order to assess the flow prediction performance of low Re YS model at the turn section, comparison with LDA measurement results from literature were needed [60]. Details are given in the APPENDIX.

4.3. Discussion and Conclusion

The present work refers to the heat transfer inside a 2 pass 1 wall ribbed channel with circular U-bend. An experimental setup for cooling channel flow and heat transfer investigations is designed and operated for the first time. The heat transfer and heat transfer enhancement results are obtained by experiments and numerical analysis are experienced using five turbulence models.

The results of experimental and numerical investigation shows that the heat transfer behaviour of a 2 pass channel shows significantly different characteristics in 1st and 2nd pass. Numerical solutions are compared with the experiments at first inter rib areas at 1st pass, U bend and downstream of the U bend of 2nd pass. In general, turbulence models come up with different results for first straight part and U turn region. Solutions for 2nd

pass are affected mostly by turning effects. Turbulence models perform in different manner at the U turn and 2nd pass when compared to 1st pass results. On the other hand, the smooth channel results show similar trend for all three turbulence models with different deviations from experimental results.

- For smooth case, heat transfer decreases along the first pass until the thermal boundary layer is developed. Turning effect gradually increases the Nusselt number level and its effect remains through the whole second pass.
- For ribbed case heat transfer inside the 1st pass show a decreasing behaviour through the channel and becomes periodical at 5th – 6th. For Re=20000 case the heat transfer enhancement along the 2nd pass reaches the developed level of 1st pass. On the other hand, flow cannot redevelop at even 21th sector and results in a constantly increasing Nu/Nu_{sm} for higher Reynolds numbers.
- Increasing the Reynolds number increases the Nusselt number everywhere, but the enhancement factor drops with increasing Reynolds number.
- The turning effect gradually increases the heat transfer for both smooth and ribbed cases through the U bend. That effect causes the abrupt decrease in the heat transfer enhancement factor starting with the bend at 11th sector (for experimental geometry).
- All v2f, YS, and RKE models give higher Nusselt number results for the smooth wall case. Among three, RKE has the closest results as it captures the heat transfer perfectly at the first pass, and gives higher Nusselt number results at the U bend section and 2nd pass.
- V2f and low Re YS models show relatively good agreement with the experimental results for ribbed case. The other turbulence models underpredict the 90 deg ribbed channel heat transfer. The heat transfer in the U bend region is overpredicted by v2f and YS models. The sudden decrease of Nu/Nu_{sm} at the U bend section is predicted larger than the experimental results.

- Regarding the turbine cooling channel, rib implementation have to be with good care because cooling channel designers have to consider the necessity of ribs and augmentation of heat transfer due to ribs.

4.4. Future Work

The flow and heat transfer at the U turn downstream region is worth to investigate deeply. In order to understand the flow and heat transfer relation at the turn and downstream of turn region deeply, a detailed numerical investigation and post processing might be performed. To come up with better predictions of heat transfer distributions, a turbulence model tuning is needed in order to compare the numerical results with experimental data confidently.

The effect of asymmetric heating might be corrected for the future measurements with the designed internal cooling experimental setup.

The heat transfer contribution of ribs at the second pass ribs might be questioned and a detailed parametric experiments or analysis might be conducted in order to see the effect of ribs on flow structure and heat transfer.

The current research is a part of an project including the development of an optimization tool. Improvement and optimization of the cooling performance is planned to be achieved adjusting the geometrical parameters like rib cross section, inter rib distance and bend geometry.

REFERENCES

- [1] H. Cohen, G. F. C. Rogers, and H. I. H. Saravanamuttoo, *Gas Turbine Theory*, 4th ed. Longman Group Limited, 1996.
- [2] R. C. Reed, *The Superalloys Fundamentals and Applications*. New York: Cambridge University Press, 2006.
- [3] J. Stringer, “The role of the coating and superalloy system in enabling advanced land-based combustion turbine development,” in *Gas Turbine Materials Technology*, 1999.
- [4] N. A. Cumpsty, *Jet Propulsion: A Simple Guide to the Aerodynamic and Thermodynamic Design and Performance of Jet Engines*. Cambridge: Cambridge University Press, 1997.
- [5] J. Han, S. Dutta, and S. V. Ekkad, *Gas Turbine Heat Transfer and Cooling*. New York: Taylor & Francis, 2000.
- [6] J. Han and J. S. Park, “Developing Heat Transfer in Rectangular Channels with Rib Tubulators,” *Int. J. Heat Mass Transf.*, vol. 31, no. 1, pp. 183–195, 1988.
- [7] J. Han, S. Ou, J. S. Park, and C. K. Lei, “Augmented Heat Transfer in Rectangular Channels of Narrow Aspect Ratios with Rib Turbulators,” *Int. J. Heat Mass Transf.*, vol. 32, no. 9, pp. 1619–1630, 1989.
- [8] J. S. Park, J. Han, Y. Huang, and S. Ou, “Heat transfer performance comparisons of five different rectangular channels with parallel angled ribs,” *Int. J. Heat Mass Transf.*, vol. 32, no. 9, pp. 2891–2903, 1992.
- [9] S. V. Ekkad and J. Han, “Detailed heat transfer distributions in two-pass square channels with rib turbulators,” vol. 40, no. 11, 1997.
- [10] M. Çakan, “Aero-thermal Investigation of Fixed Rib-roughened Internal Cooling Passages,” Universite Catholique de Louvain, 2000.
- [11] P. Vass, “Large Eddy Simulation of a Ribbed Duct Flow with FLUENT : Effect of Rib Inclination,” 2005.

- [12] J. Han, L. R. Glicksman, and W. M. Rohsenow, "An investigation of heat transfer and friction for rib-roughened surfaces," *Int. J. Heat Mass Transf.*, vol. 21, pp. 1143–1156, 1978.
- [13] Y.-H. LIU, "Effect of Rib Spacing on Heat Transfer and Friction in a Rotating Two-Pass Rectangular (AA=1:2) Channel," Texas A&M University, 2005.
- [14] J. Ahn, H. Choi, and J. S. Lee, "Large Eddy Simulation Of Flow And Heat Transfer In A Channel Roughened By Square Or Semicircle Ribs," in *Proceedings of ASME Turbo Expo 2004*, 2004.
- [15] R. Kiml, S. Mochizuki, and A. Murata, "Effects of Rib Arrangements on Heat Transfer and Flow Behavior in a Rectangular Rib-Roughened Passage : Application to Cooling," vol. 123, no. August, pp. 675–681, 2001.
- [16] J. Han, Y. Zhang, and C. P. Lee, "Augmented heat transfer in square channels with parallel, crossed and v-shaped angled ribs," *J. Heat Transfer*, vol. 113, pp. 590–596, 1991.
- [17] R. T. Kukreja, S. C. Lau, and R. D. McMillin, "Local heat/mass transfer distribution in a square channel with full and V-shaped ribs," *Int. J. Heat Mass Transf.*, vol. 36, no. 8, pp. 2013–2020, Jan. 1993.
- [18] J. Han, "Heat Transfer and Friction in Channels With Two Opposite Rib-Roughened Walls," *J. Heat Transfer*, vol. 106, no. November 1984, pp. 774–781, 1984.
- [19] M. E. Taslim, "Effects of Turbulator Profile and Spacing on Heat Transfer and Friction in a Channel," vol. 8, no. 3, pp. 555–562, 1994.
- [20] A. Layek, J. S. Saini, and S. C. Solanki, "Effect of chamfering on heat transfer and friction characteristics of solar air heater having absorber plate roughened with compound turbulators," *Renew. Energy*, vol. 34, no. 5, pp. 1292–1298, 2009.
- [21] P. Land, R. S. Bunker, and S. J. Osgood, "The Effect of Turbulator Lean on Heat Transfer and Friction in A Square Channel," pp. 1–8, 2003.
- [22] A. P. Rallabandi, H. Yang, and J. Han, "Heat Transfer and Pressure Drop Correlations for Square Channels With 45 Deg Ribs at High Reynolds Numbers," vol. 131, no. July, pp. 1–10, 2009.

- [23] R. Kamali and a. R. Binesh, “The importance of rib shape effects on the local heat transfer and flow friction characteristics of square ducts with ribbed internal surfaces,” *Int. Commun. Heat Mass Transf.*, vol. 35, no. 8, pp. 1032–1040, Oct. 2008.
- [24] L. Wang and Æ. B. Sunde, “Experimental investigation of local heat transfer in a square duct with various-shaped ribs,” pp. 759–766, 2007.
- [25] P. Agarwal, “Heat / Mass Transfer in Smooth and Ribbed Rectangular Serpentine Passages of Different Aspect Ratios and Orientation,” Louisiana State University, 2004.
- [26] R. Kiml, S. Mochizuki, A. Murata, and M. Sulitka, “Rib-Induced Secondary Flow Structures inside a High Aspect Ratio Trapezoidal Channel,” pp. 7–14, 2003.
- [27] D. K. Lezius and J. P. Johnston, “Roll-cell instabilities in rotating laminar and trubulent channel flows,” *J. Fluid Mech.*, vol. 77, no. 01, pp. 153–174, 1976.
- [28] J. H. Wagner, B. V. Johnson, and F. C. Kopper, “Heat Transfer in Rotating Serpentine Passages With Smooth Walls,” *J. Turbomach.*, vol. 113, pp. 312–330, 1991.
- [29] J. H. Wagner, B. V. Johnson, R. A. Graziani, and F. C. Yeh, “Heat Transfer in Rotating Serpentine Passages With Trips Normal to the Flow,” vol. 114, no. October 1992, pp. 847–857, 1992.
- [30] M. Rowe, “Measurements and computations of flow in pipe bends,” *J. Fluid Mech.*, vol. 43, pp. 771–783, 1970.
- [31] J. Azzola, J. A. C. Humphrey, H. Iacovides, and B. E. Launder, “Developing Turbulent Flow in a U-Bend of Circular Cross-Section : Measurement and Computation,” *J. Fluids Eng.*, vol. 108, no. June, pp. 214–221, 1986.
- [32] J. Schabacker, A. Bölcs, and B. V. Johnson, “PIV Investigation of the Flow Characteristics in an Internal Coolant Passage with Two Ducts Connected by a Sharp 180 0 Bend,” in *International Gas Turbine & Aeroengine Congress & Exhibition*, 1998.
- [33] T.-S. Wang and M. K. Chyu, “Heat convection in a 180-deg turning duct with different turn configurations,” *J. Thermophys. Heat Transf.*, vol. 8, no. 3, pp. 595–601, Jul. 1994.

- [34] M. K. Chyu, “Regional Heat Transfer and Pressure Drop in Two-Pass and Three-Pass Flow Passages with 180-Degree Sharp Turns,” in *Gas Turbine and Aeroengine Congress and Exposition*, 1989.
- [35] K. Saha and S. Acharya, “Effect of Bend Geometry on Heat Transfer and Pressure Drop in a Two-Pass Coolant Square Channel for a Turbine,” *J. Turbomach.*, vol. 135, no. March 2013, pp. 1–12, 2013.
- [36] M. Hirota, H. Fujita, A. Syuhada, S. Araki, T. Yoshida, and T. Tanaka, “Heat / mass transfer characteristics in two-pass smooth channels with a sharp 180-deg turn,” *Int. J. Heat Mass Transf.*, vol. 42, pp. 3757–3770, 1999.
- [37] W. Chen, J. Ren, and H. Jiang, “Effect of Turning Vane Configurations on Heat Transfer and Pressure Drop in a Ribbed Internal Cooling System,” *J. Turbomach.*, vol. 133, no. October, pp. 1–11, 2011.
- [38] S. Mochizuki, A. Murata, and M. Fukunaga, “Effects of Rib Arrangements on Pressure Drop and Heat Transfer in a Rib-Roughened Channel With a Sharp 180 deg Turn,” *J. Turbomach.*, vol. 119, pp. 610–616, 1997.
- [39] A. Murata and S. Mochizuki, “Large eddy simulation of turbulent heat transfer in a rotating two-pass smooth square channel with sharp 180 ° turns,” vol. 47, pp. 683–698, 2004.
- [40] A. Murata and S. Mochizuki, “Effect of rib orientation and channel rotation on turbulent heat transfer in a two-pass square channel with sharp 180 ° turns investigated by using large eddy simulation,” vol. 47, pp. 2599–2618, 2004.
- [41] C. Wang, L. Wang, and B. Sundén, “Heat transfer and pressure drop in a smooth and ribbed turn region of a two-pass channel,” *Appl. Therm. Eng.*, vol. Accepted M, 2015.
- [42] J. Kay and R. M. Nedderman, *Fluid Mechanics and Transfer Processes*. Cambridge University Press, 1985.
- [43] M. S. Bhatti and R. K. Shah, *Turbulent and Transition Flow Convective Heat Transfer in Ducts*. New York: Wiley Interscience, 1987.
- [44] W. Zhi-qing, “Study on Correction Coefficients of Laminar and TURbulent Entrance Region Effects in Round Pipes,” *Appl. Math. Mech.*, vol. 3, pp. 433, 1983, 1983.

- [45] “No Title.” [Online]. Available: <http://www.plexiglas.com/export/sites/plexiglas/.content/medias/downloads/sheet-docs/plexiglas-mc.pdf>.
- [46] “No Title.” [Online]. Available: http://www.plexiglas-shop.com/pdfs/en/211-1_PLEXIGLAS_GS_XT_en.pdf.
- [47] T.-M. Liou and J.-J. Hwang, “Effect of ridge shapes on turbulent heat transfer and friction in a rectangular channel,” *Int. J. Heat Mass Transf.*, vol. 36, no. 4, pp. 931–940, Mar. 1993.
- [48] M. E. Taslim, T. Li, and S. D. Spring, “Measurements of Heat Transfer Coefficients and Friction Factors in Passages Rib-Roughened on All Walls,” *J. Turbomach.*, vol. 120, no. July 1998, pp. 564–570, 1998.
- [49] M. E. Taslim, T. Li, and D. M. Kercher, “Experimental heat transfer and friction in channels roughened with angled, V-shaped, and discrete ribs on two opposite walls,” *Int. J. Heat Mass Transf.*, vol. 118, pp. 20–28, 1996.
- [50] K. M. Kim, H. Lee, B. S. Kim, S. Shin, D. H. Lee, and H. H. Cho, “Optimal design of angled rib turbulators in a cooling channel,” *Heat Mass Transf. und Stoffuebertragung*, vol. 45, no. 12, pp. 1617–1625, 2009.
- [51] T. Astarita and G. Cardone, “Thermofluidynamic analysis of the flow in a sharp 180° turn channel,” *Exp. Therm. Fluid Sci.*, vol. 20, pp. 188–200, 2000.
- [52] M. E. Taslim and H. Liu, “A Combined Numerical and Experimental Study of Heat Transfer in a Roughened Square Channel with 45° Ribs,” *Int. J. Rotating Mach.*, vol. 2005, no. 1, pp. 60–66, 2005.
- [53] G. Xie, S. Li, W. Zhang, and B. Sunden, “Computational Fluid Dynamics Modeling Flow Field and Side-Wall Heat Transfer in Rectangular Rib-Roughened Passages,” *J. Energy Resour. Technol.*, vol. 135, no. 4, p. 042001, 2013.
- [54] A. Inc., “ANSYS FLUENT 14.0 Theory Guide.”
- [55] H. Versteeg and W. Malalasekera, *An Introduction to Computational Fluid Dynamics: The Finite Volume Method*. New York: Longman Scientific & Technical, 1995.

- [56] B. E. Launder and D. B. Spalding, "The numerical computation of turbulent flows," *Comput. Methods Appl. Mech. Eng.*, vol. 3, no. 2, pp. 269–289, Mar. 1974.
- [57] W. R. Dean and J. M. Hurst, "Note on the motion of a fluid in a curved pipe," *Philos. Mag.*, vol. 4, no. 2, pp. 208–223, 1927.
- [58] A. Kalpakli and R. Örlü, "Turbulent pipe flow downstream a 90° pipe bend with and without superimposed swirl," *Int. J. Heat Fluid Flow*, vol. 41, pp. 103–111, 2013.
- [59] G. Rau, M. Çakan, D. Moeller, and T. Arts, "The Effect of Periodic Ribs on the Local Aerodynamic and Heat Transfer Performance of a Straight Cooling Channel," *J. Turbomach.*, vol. 120, no. 2, p. 368, 1998.
- [60] S. C. Cheah, H. Iacovides, D. C. Jackson, H. Ji, and B. E. Launder, "LDA Investigation of the Flow Development Through Rotating U-Ducts," vol. 118, no. July 1996, pp. 590–596, 2015.

APPENDIX

The smooth channel model with square cross section of Cheah et al. [60] is numerically modelled and analyzed using the low Re YS model. Description of the channel model is presented in Figure A. 1.

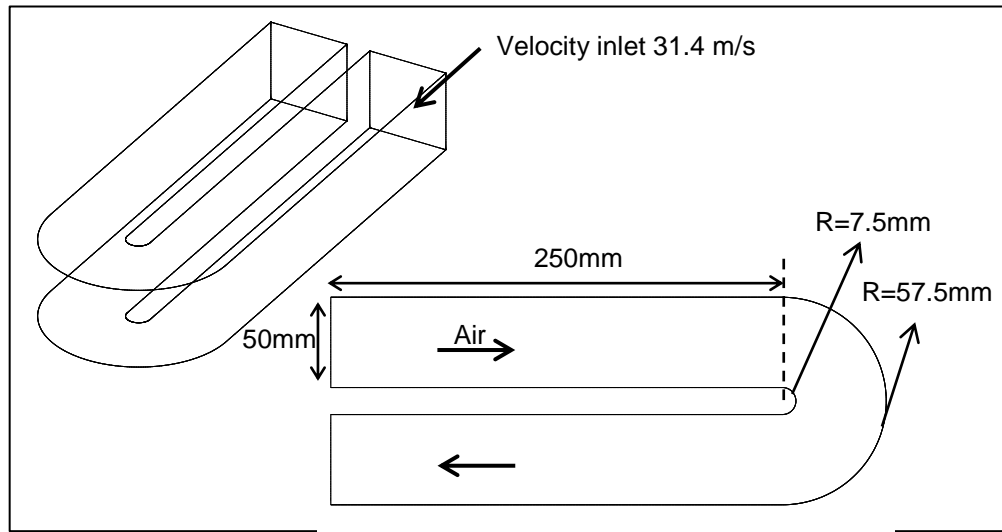


Figure A. 1 Model Description

The Reynolds number is kept 100000 the same as just as the experimental investigation [60]. Mesh structure (1.8 million) is depicted in Figure A. 2. y^+ values are kept below 2.

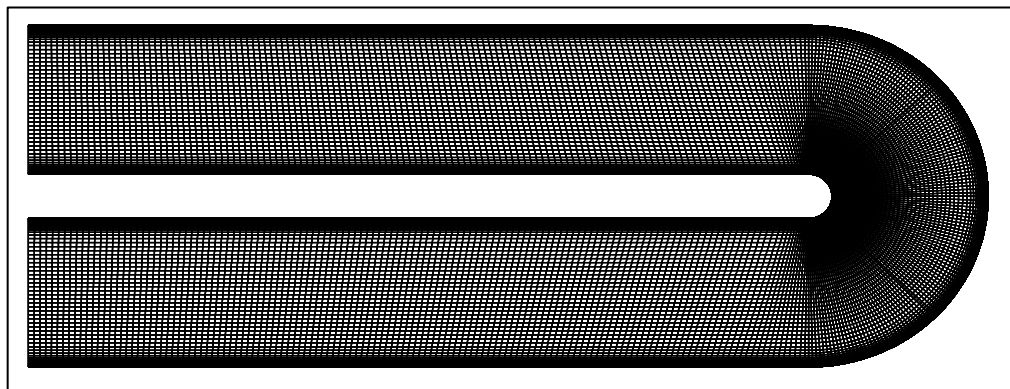


Figure A. 2 Mesh structure of the smooth model

The velocity results normalized by the streamwise velocity are compared at three locations at the bend section at 12.5% and 50% height from the channel bottom wall. The data results are extracted from the lines which are shown in Figure A. 3.

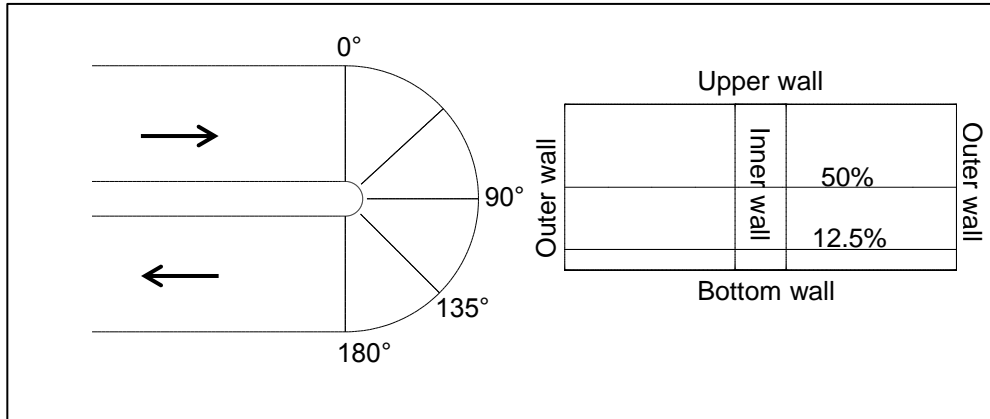


Figure A. 3 Location of measurement lines

Normalized velocity along the measurement lines are presented in Figure A. 4. At 12.5% height from the bottom wall, YS model successfully predicts the flow along the bend. However, at the channel symmetry (50% height) there is a variance between the YS model and experiment at 90°, 135°, and 180°. That gap results from the that the size of the turn induced secondary flows (Dean type) cannot be predicted successfully. The overpredicted heat transfer results at the turn and second pass of the smooth configuration can be attributed to the inadequate prediction of that secondary flows. In addition, successful prediction of flow might not give the correct heat transfer prediction since the turbulence models are established using flow parameters rather than the heat transfer.

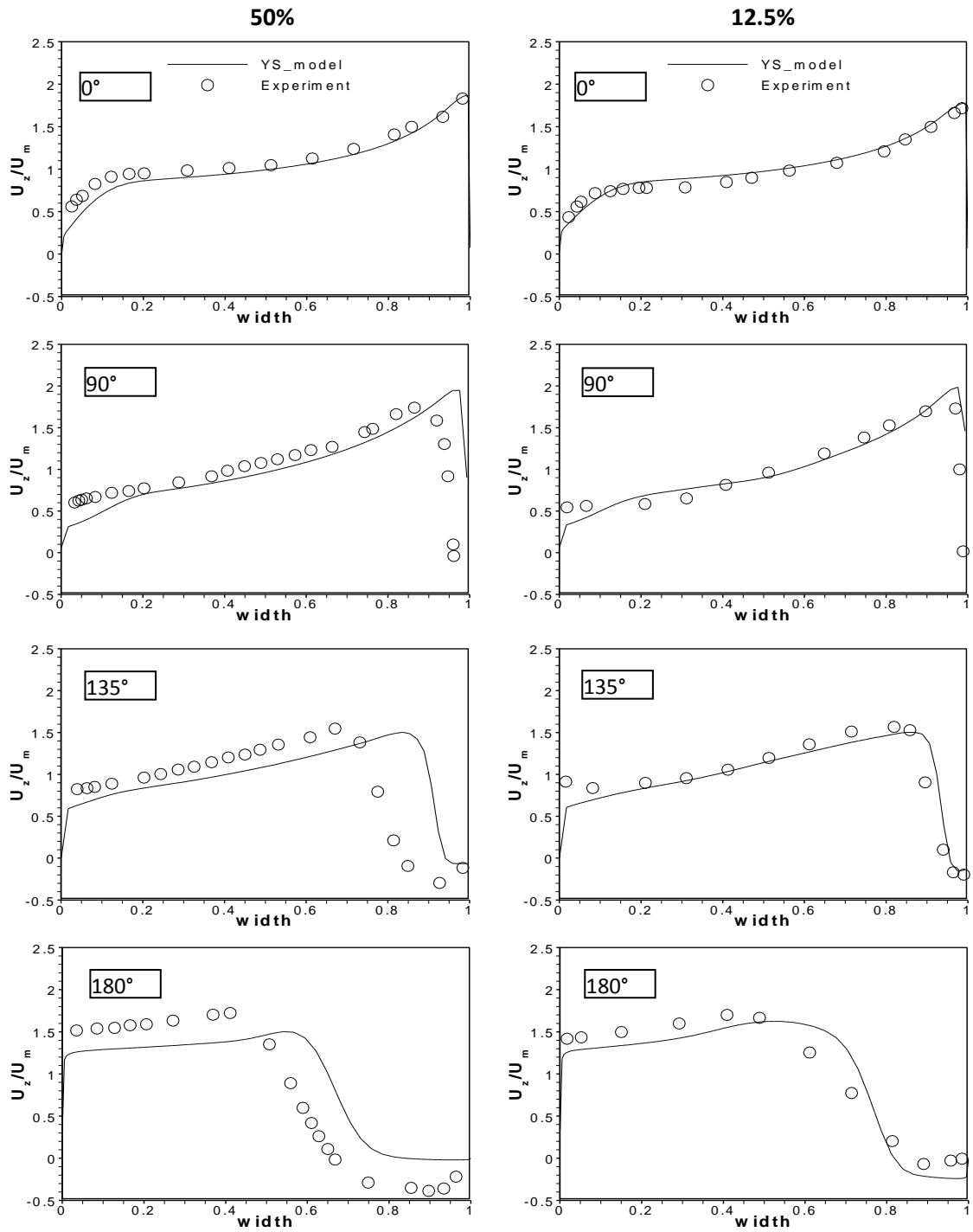


Figure A. 4 Normalized streamwise velocities along the U bend